Fatty acid-activated proton transporter SR4 prevents hepatic steatosis and metabolic alterations in diabetic mice by improving mitochondria function, energy balance and oxidative stress

JAMES FIGAROLA[1], JYOTSANA SINGHAL[1] and SHARAD SINGHAL[2]

[1]Department of Diabetes Complications and Metabolism, Arthur Riggs Diabetes and Metabolism Research Institute, City of Hope National Medical Center, Duarte, CA 91010, USA; [2]Department of Medical Oncology and Therapeutics Research, Beckman Research Institute, City of Hope National Medical Center, Duarte, CA 91010, USA

Received June 4, 2025; Accepted November 26, 2025

DOI: 10.3892/etm.2026.13190

Abstract. Type 2 diabetes (T2D) is a growing global health crisis, largely driven by rising obesity rates. Untreated T2D leads to severe complications such as cardiovascular disease, nephropathy, retinopathy, neuropathy and hepatic dysfunction. Current therapies primarily manage hyperglycemia but often fail to address core pathophysiological drivers such as insulin resistance and obesity. This highlights an urgent need for novel therapeutics with distinct mechanisms, particularly those targeting energy metabolism and insulin sensitivity, to improve long-term T2D outcomes. Modulating mitochondrial respiration through mild uncoupling has emerged as a promising strategy to promote negative energy balance. SR4, a small-molecule mitochondrial uncoupler, represents a novel class of fatty acid-activated proton transporters. In the present study, the metabolic effects of oral SR4 administration were investigated in male *db*/*db* mice, a model of T2D. SR4 significantly reduced body weight gain and improved body composition by selectively decreasing fat mass without affecting lean mass. Indirect calorimetry demonstrated that SR4 treatment increased oxygen consumption and total energy expenditure, independent of food intake. Importantly, SR4 notably improved glycemic control, reduced insulin resistance and prevented dyslipidemia, hepatic steatosis and liver injury. Mechanistically, SR4 activated hepatic AMPK, enhanced mitochondrial respiration and mitigated oxidative stress. Liver transcriptomic profiling further demonstrated broad metabolic reprogramming, including downregulation of lipogenesis and PPARγ signaling, concurrently with the upregulation of genes involved in energy metabolism and antioxidant defense. Collectively, these findings demonstrated that SR4 ameliorates multiple aspects of metabolic dysfunction in an obese T2D mouse model by targeting key pathways in energy regulation and lipid metabolism. The present results provided additional mechanistic insights into the effects of mitochondrial uncouplers in the liver and support further investigation of SR4 and related fatty acid anion transporters as a novel therapeutic class for metabolic diseases.

Correspondence to: Dr James Figarola, Department of Diabetes Complications and Metabolism, Arthur Riggs Diabetes and Metabolism Research Institute, City of Hope National Medical Center, 1500 East Duarte Road, Duarte, CA 91010, USA
E-mail: jfigarola@coh.org

Abbreviations: ACC, acetyl-CoA carboxylase; ALT, alanine transaminase; AMPK, adenosine monophosphate-activated protein kinase; AST, aspartate aminotransferase; BW, body weight; DEGs, differentially expressed genes; GSH, glutathione; GST, glutathione S-transferase; GPx, glutathione peroxidase; MASLD, metabolic dysfunction-associated steatotic liver disease; MDA, malondialdehyde; MASH, metabolic dysfunction-associated steatohepatitis; OCR, oxygen consumption rate; PPARγ, peroxisome proliferator-activated receptor γ; PPI, protein-protein interaction; PPP, pentose phosphate pathway; qPCR, quantitative PCR; T2D, type 2 diabetes; TCA, tricarboxylic acid; TG, triglycerides

Key words: mitochondria uncoupling, diabetes, obesity, steatosis, AMPK, fatty anion transporter, energy balance, metabolism, protein network, transcriptome analysis

Introduction

Type 2 diabetes (T2D) accounts for >90% of all diabetes cases and represents a rapidly escalating global health crisis (1). The 2025 International Diabetes Federation estimated that ~589 million adults worldwide are currently living with diabetes, a figure projected to rise to 853 million by 2050 (2). Globally, T2D is now the eighth leading cause of disease burden, responsible for ~6.7 million mortalities annually and is predicted to become the second leading cause of mortality by 2050 (3). Characterized by insulin resistance and impaired insulin secretion, T2D is associated with persistent hyperglycemia and is often accompanied by dyslipidemia (4) and increased oxidative stress (5). If poorly managed, T2D can lead to severe micro- and macrovascular complications, including cardiovascular disease, nephropathy, retinopathy and neuropathy, markedly reducing quality of life and escalating healthcare costs. Furthermore, ~70% of individuals with T2D are concurrently diagnosed with metabolic dysfunction-associated

steatotic liver disease (MASLD). This comorbidity markedly elevates the risk of advanced liver conditions such as metabolic dysfunction-associated steatohepatitis (MASH), cirrhosis and hepatocellular carcinoma (6,7).

Current therapeutic strategies for T2D primarily aim to mitigate hyperglycemia by enhancing insulin secretion or improving insulin sensitivity. Standard treatment regimen typically involves lifestyle modifications, oral antidiabetic agents, injectable therapies or their combination, with goals extending beyond glycemic control to address associated metabolic disturbances such as dyslipidemia and hypertension (8). However, numerous existing interventions often fall short of comprehensively addressing the complex network of underlying metabolic derangements driving T2D and its multifaceted complications.

Mitochondrial dysfunction has emerged as a central contributor to the pathogenesis of various metabolic diseases. Previous evidence indicates that inducing mild mitochondrial uncoupling can alleviate metabolic disorders by promoting energy expenditure, enhancing mitochondrial respiratory efficiency and improving insulin sensitivity and hepatic lipid metabolism (9-11). These insights have renewed a focus on developing mitochondrial uncouplers as potential therapeutic agents for T2D, obesity and MASLD. SR4 is a small-molecule mitochondrial uncoupler previously identified by our research group for its potent anticancer activity *in vitro* and in tumor xenograft models (12-14). Unlike traditional protonophore uncouplers such as carbonyl cyanide-p-trifluoromethoxyphenylhydrazone (FCCP), BAM15 and niclosamide, SR4 belongs to a newly defined class of fatty acid-activated proton transporters that facilitate the translocation of fatty acid anions across the mitochondrial inner membrane, inducing controlled proton leak and mitochondrial uncoupling (15,16). An earlier study demonstrated that SR4 improves metabolic parameters in high-fat diet (HFD)-induced obese mice, including mitigating weight gain, hyperglycemia and hepatic steatosis (17).

Over the years, numerous mouse models of obesity and diabetes have been developed, providing valuable insights into the cellular and molecular mechanisms regulating energy metabolism and homeostasis. The present study aimed to evaluate the metabolic effects of SR4 in *db/db* mice, a well-established genetic model of obesity and T2D characterized by severe, progressive hyperglycemia, insulin resistance, dyslipidemia and hepatic steatosis (18). To elucidate the mechanistic basis of SR4's action, the present study specifically focused on the liver, given its central role in energy homeostasis and nutrient metabolism.

Materials and methods

Chemicals and reagents. SR4 was previously synthesized from a validated protocol at the Chemical GMP Synthesis Facility, Beckman Research Institute of the City of Hope (CA, USA) (14). All other chemicals and reagents were purchased from Sigma-Aldrich (Merck KGaA), unless otherwise specified.

Animal studies. All animal experiments were conducted in accordance with a protocol approved by the City of Hope National Medical Center's Institutional Animal Care and Use Committee (Duarte, USA; approval no. 12004). Male 9-week-old *db/db* mice (BKS.Cg-Dock7^{m} +/+ Lepr^{db}/J) weighing 40-45 g were obtained from Jackson Laboratory. A total of 32 animals were divided into two groups: Vehicle control group and SR4-treated group; eight animals per group were used for the efficacy studies and another eight animals per group were used for the metabolic/indirect calorimetry studies. Mice were kept in specific pathogen-free conditions at 22˚C with a 12/12 h light/dark cycle. The animals had unrestricted access to water and standard chow diet (LabDiet® 5K52; Scott Distributing; ScottPharma Solutions). After 1 week of acclimatization, mice received either the vehicle control (4% DMSO in corn oil) or SR4 dissolved in vehicle (10 mg/kg of BW) via oral gavage (14). Dosing was performed three times a week (Mon, Wed and Fri) in the early morning across a 5-week period. Food consumption was monitored throughout the present study. The animals were monitored daily for health and behavior. Mice were weighed weekly and body composition (lean mass and fat mass) was measured by quantitative magnetic resonance imaging (EchoMRI™ 3-in-1; v2.1; Echo Medical Systems). All animals survived until the end of the present study and did not meet any of the humane endpoints for early euthanasia, which included failure to eat or drink for 24 h, inability to make normal posture and behavior, signs of severe distress and >20% weight loss. At study completion, mice were euthanized via CO_2 inhalation (30-70% total chamber volume/min) followed by cervical dislocation and observation of cessation of breathing to confirm mortality. Blood was then collected through cardiac puncture and the plasma was separated for subsequent analysis. Tissue samples were collected and either snap-frozen and stored at -80˚C or preserved in 10% neutral buffer formalin for further biochemical and immunohistochemical analyses, respectively.

Glucose tolerance tests. To assess glucose tolerance, mice were fasted for 16 h overnight. A 2 g/kg BW D-glucose solution was then administered intraperitoneally. Tail vein blood (~5-10 μl) was collected serially at 0, 30, 60, 90 and 120 min post-challenge through the tail-nick method (19) The blood collection procedure was approved by the Institutional Animal Care and Use Committee of City of Hope in accordance with the NIH 'Guidelines for Survival Blood Collection in Mice and Rats' (https://oacu.oir.nih.gov/). Blood glucose concentration was measured with an Accu-Chek Compact Plus glucometer (Roche Diagnostics Ltd.). The total area under the curve (AUC) was calculated using the trapezoidal method.

Indirect calorimetry. Indirect calorimetry was performed in a separate experiment using the PhenoMaster (version 5.9.3; cat. no. 2016-5420; TSE Systems) at the Comprehensive Metabolic Phenotyping Core at Beckman Research Institute (CA, USA). Mice were treated with SR4 or vehicle for 5 weeks (n=8/group). The animals were allowed to acclimate to the cages for 2 days before two cycles of 24 h measurements. Both oxygen consumption ($V0_2$) and carbon dioxide output ($VC0_2$) were normalized to lean mass as determined by EchoMRI™. The respiratory exchange ratio (RER) was calculated as $VC0_2/V0_2$. With this, the energy expenditure (EE), standardized for BW, was calculated using the following formula: $EE=(3.185 + 1.232 \times RER) \times V0_2$.

Biochemical analysis of blood and liver samples. Plasma was extracted from blood samples following centrifugation at 2,000 x g at 4˚C for 10 min. Plasma insulin was measured using a commercial kit according to the manufacturer's protocol (Crystal Chem Ultra Sensitive Mouse Insulin Elisa kit; cat. no. 90080; Crystal Chem, Inc.). Concentrations of plasma alanine transaminase (ALT), aspartate aminotransferase (AST), total triglycerides (TG) and cholesterol were quantified using commercially available kits (ALT Activity Assay Kit, cat. no. MET-512; AST Assay Kit, cat. no. MET-5127; Triglyceride Quantification kit, cat. no. STA-39; Total Cholesterol Assay Kit, cat. no. STA-384) from Cell BioLabs, Inc., according to the manufacturer's instructions. Levels of glycated hemoglobin (HbA1c) in the blood were measured using the mouse HbA1c assay kit (cat. no. 80310; Crystal Chem, Inc) according to the manufacturer's instructions. Liver TG were measured as previously described (17). Hepatic nucleotides (ATP and AMP) were measured using UV-high-performance liquid chromatography. Briefly, 100 μl of liver homogenates was removed and mixed with 100 μl of deionized water. Furthermore, 18.5 μl of 1 M potassium hydroxide, 30 μl of 150 mM monopotassium phosphate (KH_2PO_4)/150 mM potassium chloride (KCl) solution (Ph 6.0) and 0.5% acetonitrile were added. The final mixture was centrifuged at 17,000 x g for 5 min at room temperature. The supernatant was then collected and transferred to an auto-injector vial and 10 μl was injected into a Thermo ODS Hypersil™ C18 column (3 μm; 150x4.6 mm; Thermo Fisher Scientific, Inc.). Isocratic separation at 25˚C was achieved using a mobile phase consisting of 150 mM KH_2PO_4, 150 mM KCl (pH 6.0) and 0.5% acetonitrile. The flow rate was set at 0.8 ml/min and a total run time of 20 min. Nucleotides were detected by their absorbance at 260 nm using a Shimadzu SPD-40 UV-Vis detector (Shimadzu Scientific Instruments, Inc.) and compared with the elution position of standards (17).

Liver pathology and histology. At the end of the present study, the liver from each mouse was harvested and weighed. Liver samples were either flash-frozen or directly fixed in 10% formalin for downstream assays. Formalin-fixed liver samples were sectioned (5 μm) and stained with H&E for 10-15 min at room temperature. Separately, frozen liver samples from each group were embedded in OCT compound (Sakura Finetek USA, Inc.), sliced and stained with Oil Red O (Sigma-Aldrich; Merck KGaA) at room temperature for 15 min. All stained slides were viewed and images were captured under a bright field microscope (cat. no. AX70; Olympus Corporation) equipped with a digital camera.

Analysis of liver oxidative stress and antioxidant activity. Multiple enzymes associated with oxidative stress and antioxidant defense, including glutathione (GSH), glutathione S-transferase (GST) and glutathione peroxidase (GPx), were measured in liver crude homogenates using established methods as previously described (20). The level of malondialdehyde (MDA), a marker of lipid peroxidation, was quantified using the thiobarbituric acid reactive substances assay as described previously (21).

Liver mitochondria isolation and bioenergetic analysis. Fresh mitochondria were isolated from the livers of mice (n=4-5/group) as described previously (12). Briefly, mice were euthanized by CO_2 inhalation and cervical dislocation as aforementioned, before livers were immediately removed, minced and placed in ~10-fold volume of ice-cold mitochondria isolation medium [250 mM sucrose, 10 mM Tris/hydrogen chloride (HCl), 1 mM EGTA and 1% fatty acid/endotoxin-free BSA; pH 7.4]. Tissues were homogenized with 25-30 strokes in a Potter-Elvehjem tissue grinder (Sigma-Aldrich; Merck KGaA). After centrifugation at 800 x g for 10 min at 4˚C, the fats and lipids were carefully aspirated. The remaining supernatant was then filtered through a sterile 0.40 μm nylon mesh membrane and centrifuged at 8,000 x g for 10 min at 4˚C. The supernatant and any white debris were removed. The mitochondrial pellet was resuspended in ice-cold mitochondrial assay solution (MAS buffer; 70 mm sucrose, 220 mM mannitol, 10 mM KH_2PO4, 5 mm magnesium chloride, 2 mM HEPES, 1 mM EGTA and 0.2% fatty acid-free BSA; pH 7.2) and this centrifugation was repeated. The final pellet was resuspended in a minimal volume of MAS buffer. Mitochondrial protein concentration was measured using the DC protein assay kit according to the manufacturer's protocol (Bio-Rad Laboratories, Inc.) with BSA as a standard. Isolated liver mitochondria were seeded at 1 μg/well in a Seahorse 96-well plate. Basal respiration (mitochondrial respiration state 2), ADP-stimulated respiration (mitochondrial respiration state 3), non-ADP-stimulated respiration (mitochondrial respiration state 4; proton leak), FCCP-stimulated respiration (mitochondrial respiration state 3u; maximal respiration) and spare respiratory capacity (SRC) were quantified using a Seahorse XF96 flux analyzer (Seahorse Biosciences, Inc.) as described previously (22).

Protein extraction and western blotting. Liver tissue samples were homogenized in a lysis buffer containing 50 mM Tris/HCl (pH 7.4), 150 mM sodium chloride, 1 mM EDTA, 5 mM sodium pyrophosphate, 1 mM sodium orthovanadate, 50 mM sodium fluoride, 1% NP-40, 1 mM PMSF and a protease inhibitor cocktail tablet (Roche Diagnostics Ltd.). Homogenates were then centrifuged for 15 min at 9,600 x g at 4˚C and supernatants were collected. Protein concentration was determined using a DC protein assay kit according to the manufacturer's instructions. For western blotting, 10 μg of protein per sample were resolved by SDS-PAGE on 4-15% Criterion TGX™ gels (Bio-Rad Laboratories, Inc.) and then transferred to nitrocellulose membranes. Membranes were blocked with 5% skimmed milk in Tris-buffered saline containing 0.05% Tween 20 for 1 h at room temperature before overnight incubation at 4˚C with a 1:1,000 dilution of primary antibodies against total and phosphorylated AMPK and total and phosphorylated ACC (cat. nos. 2532, 2537, 8578 and 3661; Cell Signaling Technology, Inc.). After a series of washes, the membranes were stained with a 1:3,000 dilution of peroxidase-labeled secondary antibodies (goat anti-rabbit IgG HRP conjugate; cat. no. 1706515; Bio-Rad Laboratories, Inc.) at room temperature for 2 h, and an ECL system (Western Lightning® Chemiluminescence Reagent; cat. no. NEL104001EA; Revvity, Inc.) was used to visualize the immunoreactive proteins. Equal loading of proteins

was confirmed by stripping and reprobing the membranes with β-actin antibodies (1:3,000 dilution; cat. no. 3700; Cell Signaling Technology, Inc.).

Quantitative PCR (qPCR). Total RNA was isolated from liver samples using the RNeasy kit (Qiagen, Inc.) according to the manufacturer's instructions. Complementary DNA (cDNA) was synthesized from the isolated RNA using the High-Capacity cDNA Reverse Transcription Kit (Thermo Fisher Scientific, Inc.). qPCR was performed on an ABI-7500 PCR system (Thermo Fisher Scientific, Inc.) using Power SYBR® Green master mix (Thermo Fisher Scientific, Inc.) for gene amplification and detection. The list of primer pairs used in the present study and their sequences are listed in Table I. The following thermocycling conditions were used for the PCR: Initial denaturation at 50˚C for 2 min; cDNA was denatured at 95˚C for 10 min; and 40 cycles 95˚C for 15 sec and 60˚C for 60 sec. The relative mRNA levels of all the target genes were quantified using the comparative $2^{-\Delta\Delta Cq}$ method with β-actin as an internal control (23).

Transcriptome analysis of whole liver. Total RNA was extracted from liver tissue samples (n=3 control and n=2 SR4 treatment) using the RNeasy Mini Kit (Qiagen, Inc.), per the manufacturer's protocol. RNA libraries were prepared using the TruSeq Stranded mRNA Library Prep Kit (Illumina, Inc.) and sequenced on the HiSeq® 2500 platform (Illumina, Inc), generating single-end 51 bp reads. Sequence alignment to the mouse reference genome (GRCm38/mm10) was performed using TopHat2(version 2.1.1; http://ccb.jhu.edu/software/tophat/index.shtml). Read quantification and normalization utilized the 'Empirical Analysis of Digital Gene Expression in R' ('edgeR'; version 4.1) package (24), based on raw count data. Differentially expressed genes (DEGs) analysis was conducted using the 'DESeq2' package (25), applying the Benjamini-Hochberg method to control the false discovery rate (FDR). Genes with an FDR<0.05 and an absolute fold change (FC) ≥1.5 were considered DEGs. A volcano plot was generated using VolcaNoseR (version v1.0.3; https://huygens.science.uva.nl/VolcaNoseR/), with Manhattan distance used to identify the top 10 DEGs (26).

Functional enrichment analysis of DEGs was performed using the Database for Annotation, Visualization and Integrated Discovery platform, version 6.8 (27), incorporating Gene Ontology (GO; https://geneontology.org/) biological processes and Kyoto Encyclopedia of Genes and Genomes (KEGG; https://www.kegg.jp) pathway annotations. Significant enrichment was defined by adjusted P<0.05 and gene counts ≥3. Furthermore, visualization was conducted using SRplot (https://www.bioinformatics.com.cn/en). To explore protein-protein interactions (PPIs), a PPI network was constructed using the STRING database (version 12.0; https://string-db.org/) (28), with a minimum confidence score of 0.7. Evidence channels for the interactions included in the network were derived from experimental data, curated databases, co-expression, gene fusion, co-occurrence, neighborhood and text mining. The resulting network was visualized and analyzed in Cytoscape (version 3.10.3; https://cytoscape.org/) (29). Significant network modules were identified using the 'Molecular Complex Detection' ('MCODE') Cytoscape plugin (30), with the following parameters: K-core=2, maximum depth=100, node score cut-off=0.2 and degree cut-off=2. Module functional annotation was further analyzed using STRING. Finally, hub genes within the PPI network were identified using the Maximal Clique Centrality (MCC) algorithm in the 'cytoHubba' plugin (31).

Table I. Primer sequences used for qPCR.

Gene	Sequence (5'-3')
Acaca	F: CCTCCGTCAGCTCAGATACA
	R: TTTACTAGGTGCAAGCCAGACA
Acly	F: AGGAAGTGCCACCTCCAACAGT
	R: CGCTCATCACAGATGCTGGTCA
β-actin	F: ACCTTCTACAATGAGCTGCG
	R: CTGGATGGCTACGTACATGG
Cebpa	F: GCAAAGCCAAGAAGTCGGTGGA
	R: CCTTCTGTTGCGTCTCCACGTT
Fasn	F: GCGATGAAGAGCATGGTTTAG
	R: GGCTCAAGGGTTCCATGTT
Pparg	F: GCCCTTTGGTGACTTTATGGA
	R: GCAGCAGGTTGTCTTGGATG
Scd1	F: CTGTACGGGATCATACTGGTTC
	R: GCCGTGCCTTGTAAGTTCTG
Srebf1	F: ATCCAGGTCAGCTTGTTTGCGATG
	R: TGGACTACTAGTGTTGGCCTGCTT

F, forward; R, reverse; *Acaca*, acetyl-coenzyme A carboxylase; *Acly*, ATP citrate lyase; *Cebpa*, CCAAT/enhancer-binding protein a; *Fasn*, fatty acid synthase; *Pparg*, peroxisome proliferator-activated receptor gamma; *Scd1*, stearoyl-coenzyme A desaturase 1; *Srebf1*, sterol regulatory element binding protein-1c.

Statistical analysis. Statistical analyses were performed using GraphPad Prism (version 10.3.1; GraphPad; Dotmatics). Data are presented as mean ± SEM. BW changes were compared between groups using repeated measure two-way ANOVA coupled with post hoc Tukey's test. Comparison between two groups was analyzed by Welch's t-test to adjust for unequal sizes and variances between samples. P<0.05 was considered to indicate a statistically significant difference.

Results

SR4 reduces BW and body fat mass without altering food intake in db/db mice. To investigate the effects of SR4 in diabetic mice, either vehicle control (4% DMSO in corn oil) or SR4 was administered through oral gavage to male *db/db* mice three times a week for 5 weeks. SR4-treated mice showed significant weight loss after only 3 weeks of treatment and at the end of the present study these animals exhibited ~13% overall weight loss compared with vehicle control (50.4±0.4 vs. 57.7±0.5 g, respectively; Fig. 1A and B). In addition, SR4-treated animals displayed a greater reduction in fat mass without any marked change in lean mass (Fig. 1C). Notably, the decrease in BW and improvement in body mass composition were not associated

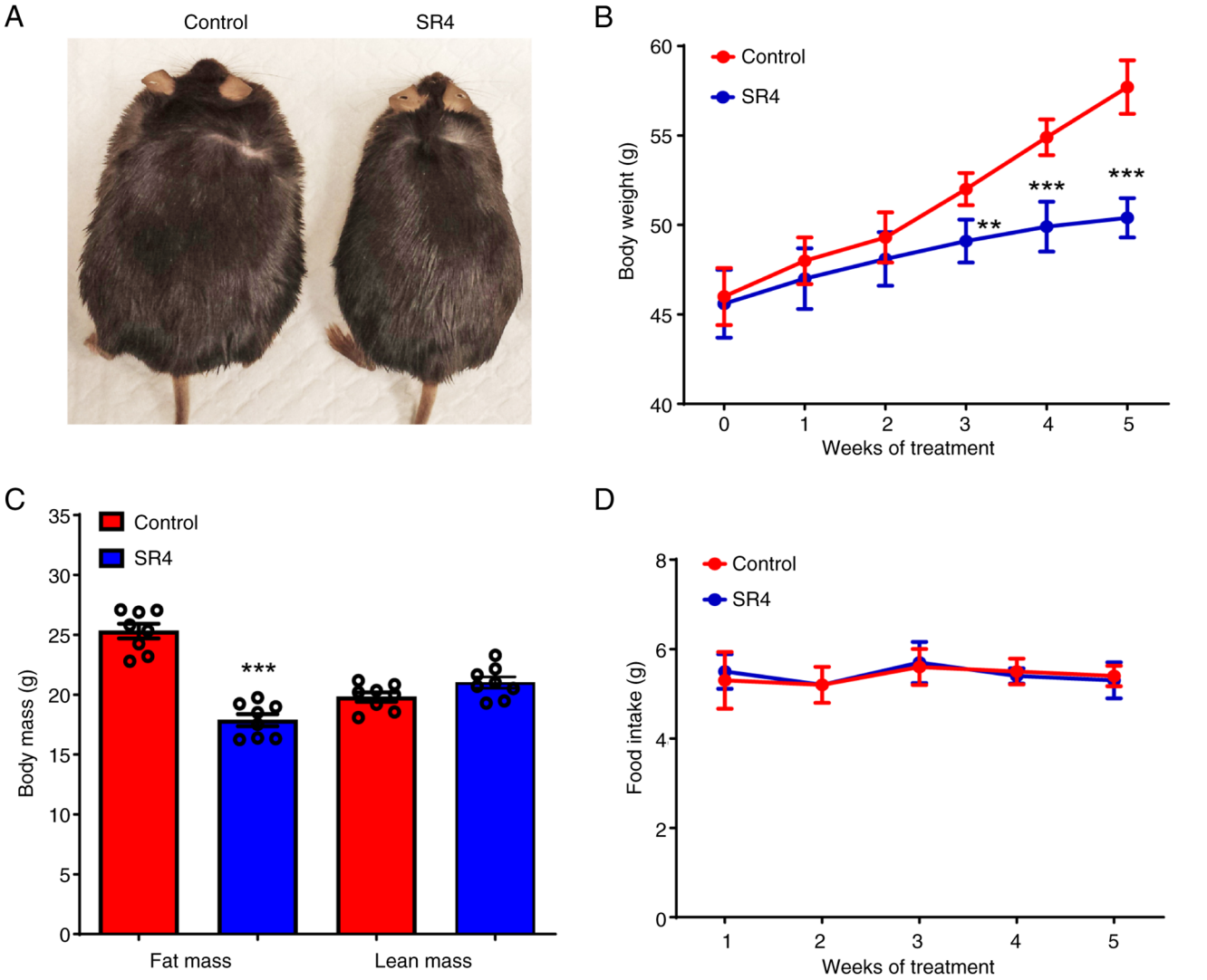

Figure 1. SR4 reduces BW and body fat mass without altering food intake in *db/db* mice. (A) Representative images of mice from each treatment group, demonstrating differences in overall body shape. (B) Weekly mean BW of vehicle vs. SR4-treated mice. (C) Quantification of body fat mass and lean mass percentage after 5 weeks of treatment, determined using EchoMRI™ technology. (D) Mean food intake of each mouse was manually measured. All quantitative data are presented as the mean ± SEM, with n=8 animals per group. Statistical significance is indicated as follows: **P<0.01 and ***P<0.001 for SR4 vs. control. BW, body weight.

with less food consumption as both SR4 treatment and control demonstrated similar daily food intake (Fig. 1D).

SR4 increases oxygen consumption and energy expenditure in db/db mice. To determine if the reductions in weight and improved body composition by SR4 was associated with energy expenditure, indirect calorimetry experiments were performed over a 3-day period (with one day acclimation). Both oxygen consumption and total daily expenditure, but not RER, were significantly increased in animals treated with SR4 compared with the control (Fig. 2A-C). Notably, the apparent increase in oxygen consumption and energy expenditure were only detected in the dark phase and not in the light phase (Fig. 2D and E). No significant change was observed in the daily RER in both dark and light cycles between SR4 and control animals (Fig. 2F).

SR4 improves glycemic control and insulin sensitivity in db/db mice. *Db/db* mice are characterized by a non-functional leptin receptor, leading to obesity and insulin resistance and ultimately causing hyperglycemia. This hyperglycemia develops progressively, with initial insulin resistance followed by a decrease in insulin secretion, resulting in sustained high blood glucose levels (32). As obesity is one of the key risk factors for insulin resistance in *db/db* mice, the effects of SR4 on glucose and insulin sensitivity were investigated. SR4 treatment significantly reduced fasting blood glucose after 5 weeks of treatment, with mean plasma glucose of 280.2±0.2 mg/dl in the control group vs. 245±0.4 mg/dl in the SR4-treated group (Fig. 3A). Similarly, HbA1c levels were also significantly decreased by SR4 at the end of treatment (Fig. 3B). Additionally, SR4 reduced the plasma insulin levels significantly (Fig. 3C). To further investigate the effects of SR4 on hyperglycemia, intraperitoneal glucose tolerance tests were performed after a 16 h fast. Glucose tolerance was quantified as the AUC integrated from 0-120 min. Control *db/db* mice exhibited impaired glucose tolerance and SR4 treatment significantly reduced the peak glucose levels after the glucose load (Fig. 3D). Consequently, glucose AUC was

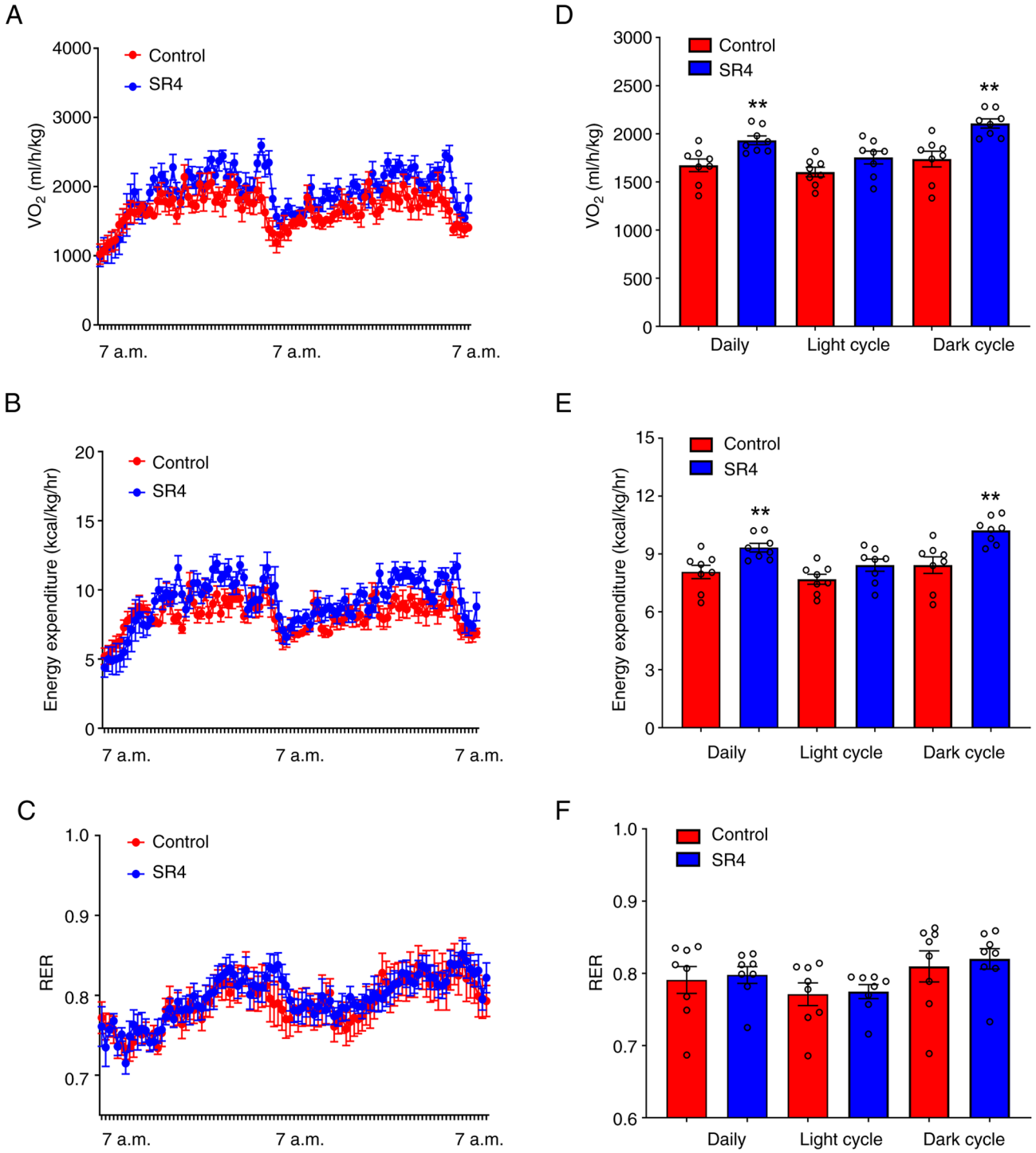

Figure 2. SR4 increases oxygen consumption and energy expenditure in *db/db* mice. (A) Daily total oxygen consumption rates, (B) energy expenditure and (C) RER of control and SR4-treated mice. (D) Average oxygen consumption, (E) energy expenditure and (F) RER in both light and dark cycles. All quantitative data are presented as the mean ± SEM, with n=8 animals per group. Statistical significance is indicated as follows: **P<0.01 for SR4 vs. control. RER, respiratory exchange ratio; VO_2, maximal oxygen consumption.

significantly suppressed in SR4-treated mice compared with control (Fig. 3E). Together, these results indicated that SR4 could improve glycemic control and insulin sensitivity in *db/db* mice.

SR4 prevents dyslipidemia, hepatic steatosis and liver injury in db/db mice. Plasma TG levels of SR4-treated mice were lower by 28% compared with that of the vehicle control group (168.1±12.8 vs. 235.8±9.0 mg/dl; Fig. 4A). SR4 also significantly decreased total cholesterol by 29% compared with control (139.6±18.2 vs. 196.5±14.3 mg/dl; Fig. 4B). As T2D is associated with the development of fatty liver in the *db/db* mice (33), the liver pathology was next examined upon SR4 treatment. Compared with the control group, SR4 treated mice had 30% lower liver wet weight (3.6±0.2 vs. 2.5±0.2 g; Fig. 4C). Biochemical analyses also revealed that SR4 significantly

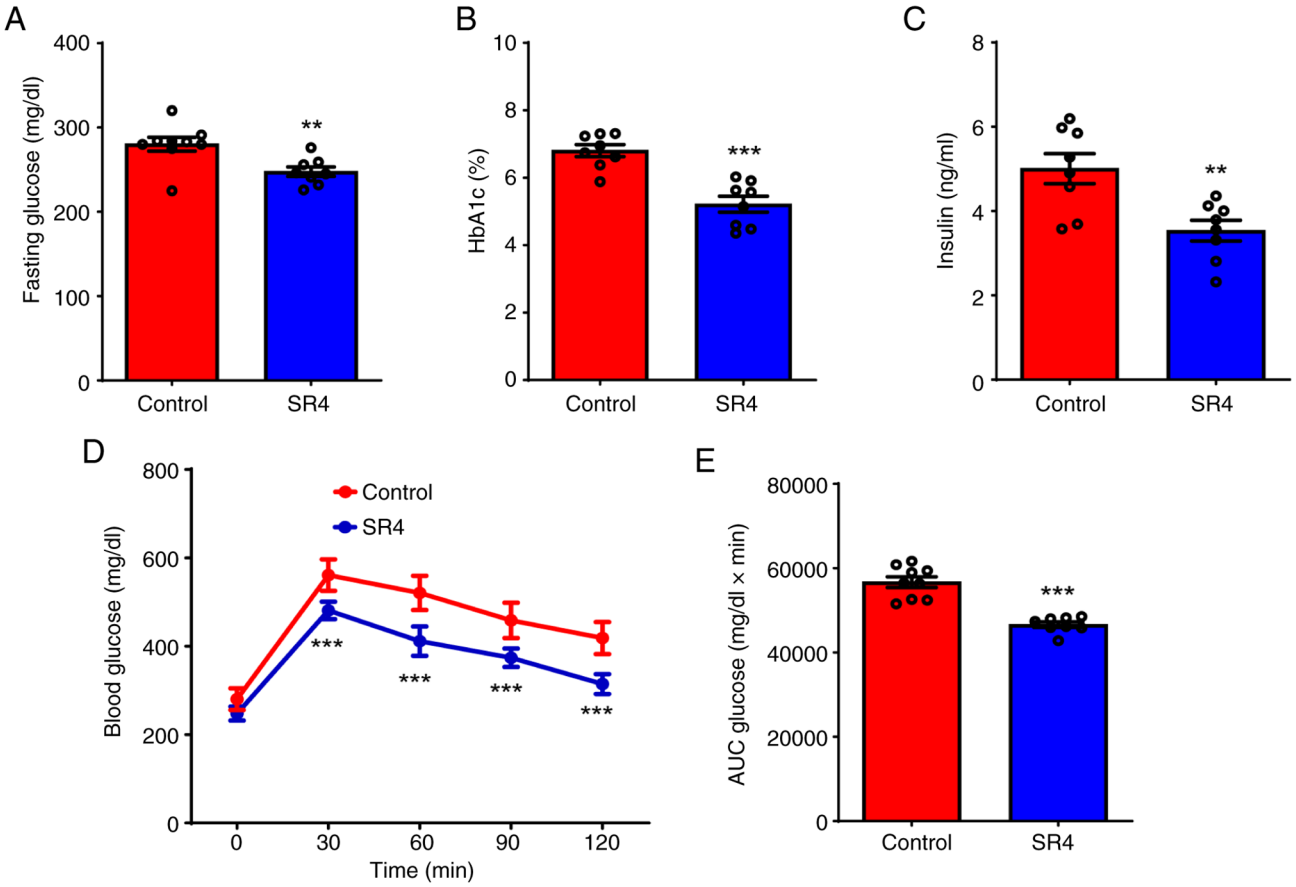

Figure 3. SR4 improves glycemic control in *db/db* mice. (A) Fasting plasma glucose, (B) HbA1c, (C) fasting plasma insulin, (D) intraperitoneal glucose tolerance test and (E) total AUC. All quantitative data are presented as the mean ± SEM, with n=8 animals per group. Statistical significance is indicated as follows: **P<0.01 and ***P<0.001 for SR4 vs. control. HbA1c, glycated hemoglobin; AUC, area under the curve.

decreased hepatic TG contents by 32% compared with control animals (78.6±4.1 vs. 116.0±2.8 mg/g protein; Fig. 4D).

Liver tissues were further analyzed to observe changes in lipid accumulation. H&E staining of liver sections revealed that *db/db* control animals exhibited numerous large vacuoles filled with excess lipids, which is characteristic of the hepatic steatosis that develops in these mice (Fig. 4E, upper panel). In addition, Oil Red O staining demonstrated an accumulation of numerous larger fat droplets in these mice (Fig. 4E, lower panel). In the SR4-treated group, hepatocellular vacuolation was minimally observed and a notable improvement in lipid accumulation with a marked reduction in the number and size of lipid droplets was detected in the liver of these animals. To determine the molecular mechanisms involved in the inhibitory effect of SR4 on hepatic steatosis, the expression of numerous known hepatic genes was measured genes using qPCR. SR4 significantly suppressed the expression of a number of genes involved in fatty acid and cholesterol synthesis, including acetyl-CoA carboxylase (ACC; *Acaca*), ATP citrate lyase (*Acly*), CCAAT/enhancer-binding protein α (*Cebpa*), fatty acid synthase (*Fasn*), PPARγ (*Pparg*), sterol regulatory element binding protein-1c (*Srebf1*) and stearoyl-coenzyme A desaturase 1 (*Scd1*; Fig. 4F). Excessive lipid accumulation in the liver is often associated with liver damage, including elevated levels of liver enzymes ALT and AST. SR4 treatment significantly decreased the plasma levels of these enzymes by 40 and 37%, respectively, compared with the control group (Fig. 4G and H). These results indicated that SR4 improved the overall pathology of the liver and attenuated the obesity-induced hepatic steatosis and liver injury in *db/db* mice.

SR4 activates hepatic AMPK, increases mitochondria respiration and prevents oxidative stress in db/db mice. Mitochondrial uncouplers such as SR4 are known to activate AMPK by disrupting mitochondrial function and reducing ATP production, which can lead to an increase in the AMP:ATP ratio, a key signal for AMPK activation (12). Chronic treatment with SR4 *in db/db* mice led to a significant increase in the hepatic AMP:ATP ratio (Fig. 5A) as well as an increase in phosphorylation of AMPK and its downstream target ACC (Fig. 5B).

An additional known effect of mitochondria uncouplers is to increase oxygen consumption and mitochondria respiration (9,12,15). Therefore, the mechanisms by which SR4 treatment can affect liver mitochondria function and bioenergetics using the Seahorse flux analyzer were examined (Fig. 5C). Mitochondria freshly isolated from the livers of mice treated with SR4 showed an increase in basal respiration (state 2) of 19.0% compared with control. Similarly, ADP-linked respiration (state 3) increased to ~80% while maximal respiration (state 3u) further increased to 120%, demonstrating increased levels of oxygen consumption linked to ATP production (Fig. 5C). This increase in oxygen

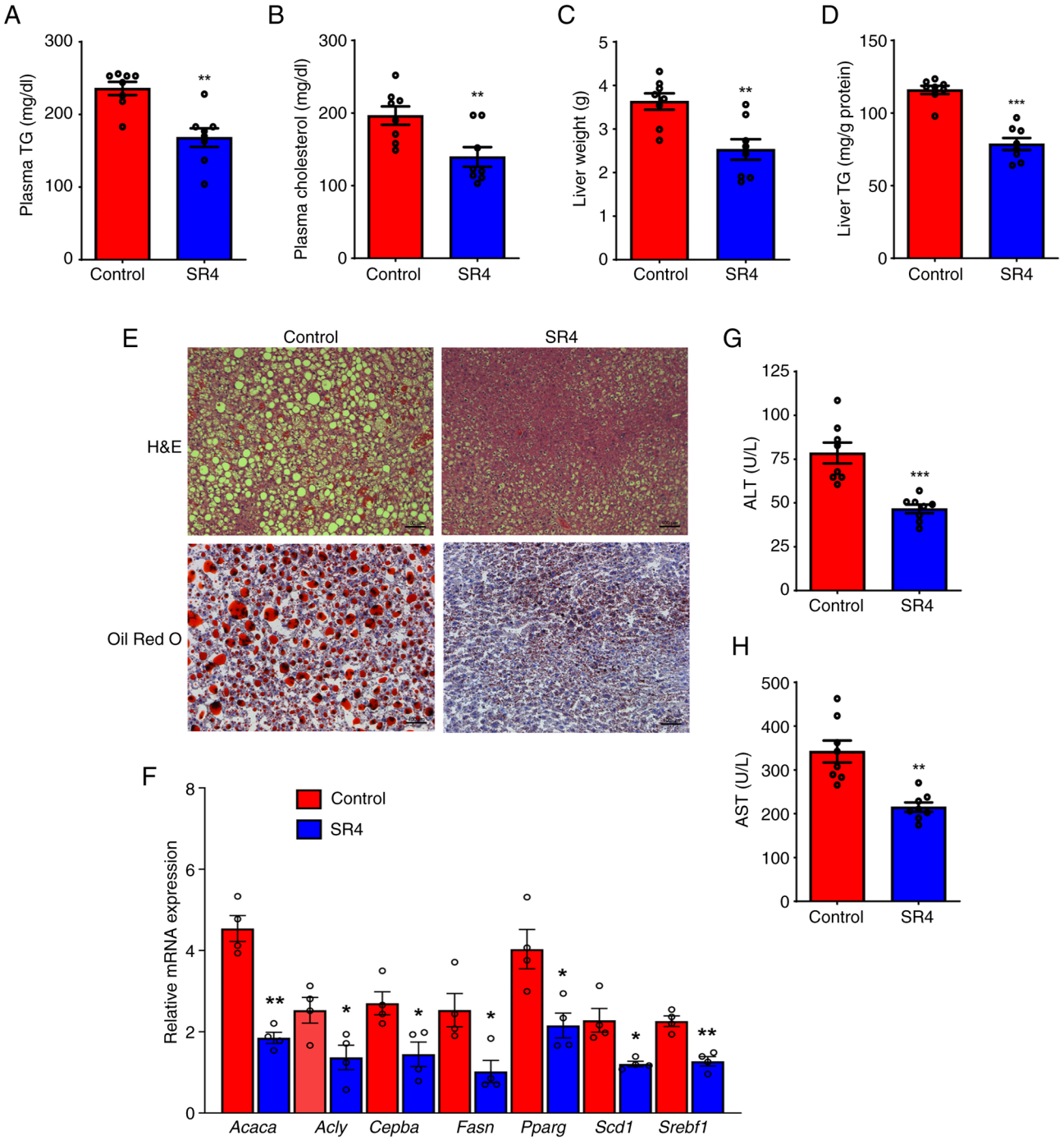

Figure 4. SR4 ameliorates dyslipidemia and hepatic steatosis in *db/db* mice. Plasma (A) TG and (B) cholesterol levels, (C) liver weight and liver TG content (D) of control and SR4-treated mice at the end of the present study. (E) Representative images of liver sections stained with H&E and Oil Red O. Magnification, x160, scale bar 100 μm. (F) Quantitative PCR analysis showing the relative mRNA expression levels of lipid metabolism-associated genes *Acaca*, *Acly*, *Cebpa*, *Fasn*, *Pparg*, *Scd1* and *Srepbf1* in liver of mice with and without SR4 treatment. Plasma levels of liver injury enzymes (G) ALT and (H) AST. All quantitative data are presented as the mean ± SEM, with n=8 animals per group for panels A-D and G-H and n=4 animals per group for panel F. Statistical significance is indicated as follows: *P<0.05, **P<0.01 and ***P<0.001 for SR4 vs. control. ALT, alanine transaminase; AST, aspartate aminotransferase; *Acaca*, acetyl-coenzyme A carboxylase; *Acly*, ATP citrate lyase; *Cebpa*, CCAAT/enhancer-binding protein a; *Fasn*, fatty acid synthase; *Pparg*, peroxisome proliferator-activated receptor g; *Scd1*, stearoyl-coenzyme A desaturase 1; *Srebf1*, sterol regulatory element binding protein-1c; TG, triglycerides.

consumption rate (OCR) further coincides with a 40% increase in proton leak across the inner mitochondrial membrane. Furthermore, SR4-treatment significantly increased the SRC, the capability to increase energy production when faced with higher demands and often used as a parameter in assessing mitochondria function, by ~195% (Fig. 5D). A previous study showed that impaired mitochondrial function in *db/db* mice can lead to oxidative stress (5). Next, the effects of SR4 on liver oxidative stress and GSH-linked antioxidant system were examined. Hepatic TBAR levels of mice treated with SR4 were lower by 53% compared with those of the control group (8.6±0.45 nmol MDA/mg protein vs. 17.9±1.45 nmol MDA/mg protein; Fig. 5E). Concomitantly, the activity levels of antioxidant enzymes GSH, GST and GPx were significantly higher

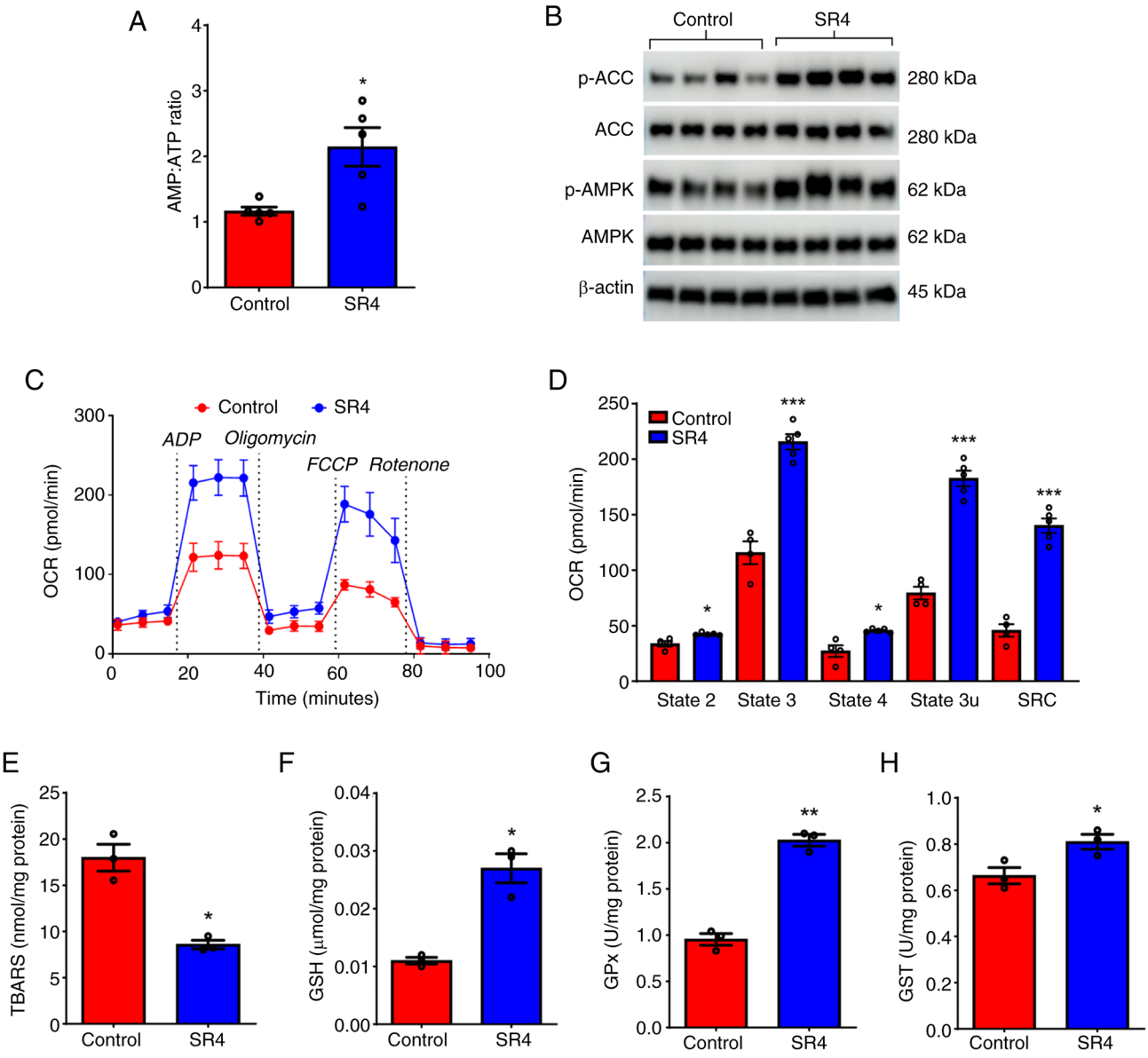

Figure 5. SR4 activates hepatic AMPK, increases liver mitochondrial respiration and alleviates oxidative stress in *db/db* mice. (A) Liver AMP:ATP ratio in control and SR4-treated animals (n=5). (B) Representative western blotting analysis of protein lysates from liver (n=3). Lysates were subjected to SDS-PAGE and immuno-blotted with antibodies specific to phosphorylated and total AMPK, phosphorylated and total ACC or β-actin. (C) Seahorse analysis of mitochondrial function and bioenergetics of freshly isolated liver mitochondria (n=4-5 per group) after 5 weeks of SR4 treatment. Real time OCR and key respiration parameters such as (D) basal respiration (state 2), ADP-linked respiration (state 3), maximal respiration (state 3u), proton leak (state 4) and spare respiratory capacity are shown. (E) Hepatic levels of MDA, measured as TBARS and antioxidants (F) GSH, (G) GPx and (H) GST in liver lysates of control and SR4-treated mice (n=3). Statistical significance is indicated as follows: *P<0.05, **P<0.01 and ***P<0.001 for SR4 vs. control. p-, phosphorylated. ACC, acetyl-CoA carboxylase; OCR, oxygen consumption rate; MDA, malondialdehyde; FCCP, carbonyl cyanide-p-trifluoromethoxyphenylhydrazone; GSH, glutathione; GST, glutathione S-transferase; GPx, glutathione peroxidase; TBARS, thiobarbituric acid reactive substances.

in the liver of SR4-treated mice compared with the control (Fig. 5F-H). Together, these data suggest that SR4 uncoupling activity could activate hepatic AMPK, improve mitochondria function and alleviate oxidative stress.

SR4 alters the expression of metabolic genes associated with key pathways regulating lipid metabolism, energy homeostasis and oxidative stress. To further investigate the effects of SR4 treatment on liver function and metabolic signaling pathways, untargeted whole-transcriptome sequencing of liver tissues isolated from *db/db* mice treated with or without SR4 was performed. This analysis identified 642 DEGs, with 217 being upregulated and 425 downregulated by SR4 treatment. Fig. 6A presents a volcano plot highlighting these DEGs based on significance criteria (adjusted P<0.05 and absolute FC≥1.5). The top 10 most strongly regulated genes included the elongation of very long chain fatty acids protein 6 (*Elovl6*), ephrin type-B receptor 2, cell death-inducing DFFA-like effector A, malic enzyme 1, arrestin domain-containing 3, fatty acid synthase (*Fasn*), ACC a (*Acaca*), cytochrome P450 3A41A, cytochrome P450 4A12B and metallothionein 1. The functional relevance of these DEGs to metabolic liver diseases, including diabetes, obesity and hepatic steatosis, is summarized in Table II (34-53). Overall, the genes most highly modulated by

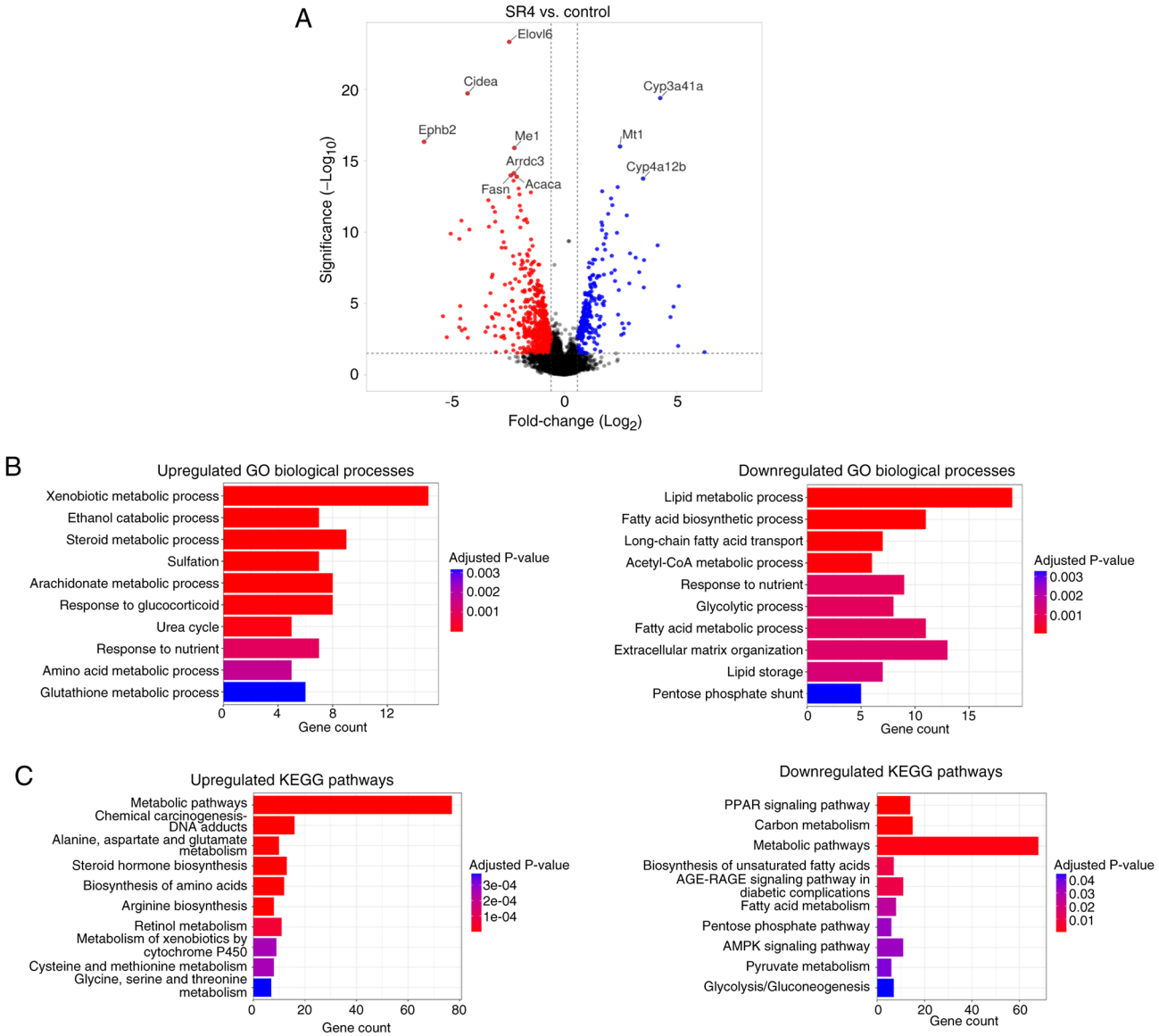

Figure 6. Transcriptomic analysis of hepatic gene expression in SR4-treated *db/db* mice. (A) Volcano plot of DEGs between SR4 and vehicle-treated *db/db* mice. DEGs with P<0.05 and a fold-change ≥1.5 are depicted in red (downregulated) and blue (upregulated) circles. Black circles represent DEGs below the cut-off. Annotated dots correspond to the top 10 DEGs with the largest (Manhattan) distance from the origin above the significance thresholds indicated by the dashed line. Data plotted using the VolcaNoseR web tool. (B) Bar plots of the top ten significantly enriched upregulated (left panel) and downregulated (right panel) GO biological processes. (C) Bar plots of the top ten significantly enriched upregulated (left panel) and downregulated (right panel) KEGG pathways. GO, gene ontology; KEGG, Kyoto Encyclopedia of Genes and Genomes.

SR4 were primarily associated with fatty acid synthesis, lipid accumulation and liver steatosis, inflammatory responses and fibrotic processes, which suggested that SR4 may exert protective effects through the coordinated regulation of hepatic metabolic and stress-response pathways.

To evaluate the biological significance of the DEGs, GO and KEGG pathway enrichment analyses were performed. GO biological process analysis indicated that the 217 upregulated DEGs were significantly enriched in pathways related to 'Xenobiotic metabolic process', 'Steroid metabolic process', 'Amino acid metabolic process', 'Urea cycle' and 'Glutathione metabolic process' (Fig. 6B). By contrast, the 425 downregulated DEGs were primarily associated with 'Lipid metabolic process', 'Fatty acid biosynthetic process', 'Lipid storage', 'Glycolytic process' and the 'Pentose phosphate shunt'. KEGG pathway analysis revealed that upregulated DEGs were enriched in 'Metabolic pathways', 'Alanine, aspartate and glutamate metabolism', 'Chemical carcinogenesis-DNA adducts', 'Steroid hormone biosynthesis', 'Biosynthesis of amino acids', 'Retinol metabolism' and 'Metabolism of xenobiotics by cytochrome P450' (Fig. 6C). Downregulated DEGs were significantly associated with the 'PPAR signaling pathway', 'Carbon metabolism', 'Fatty acid metabolism', 'AMPK signaling pathway', 'Glycolysis/Gluconeogenesis' and the 'Pentose phosphate pathway'. These results indicated that the transcriptional changes induced by SR4 treatment involve key pathways regulating nutrient metabolism, energy homeostasis and oxidative stress, processes that are involved in the pathogenesis of T2D and progression to MASLD.

To assess the functional relationships among the identified DEGs, a PPI network was constructed using

Table II. Top 10 transcripts regulated by SR4 treatment in the liver of *db*/*db* mice and their functions and association with liver metabolic diseases, diabetes and obesity.

Gene	Effect of SR4	Gene function and association	(Refs.)
Elovl6	Downregulated	*Elovl6* encodes fatty acid elongase 6, an enzyme primarily involved in the elongation of C12-C16 saturated and monounsaturated fatty acids to C18 species. Hepatic *Elovl6* expression is highly upregulated in genetically obese mouse models, such as *ob*/*ob* and *db*/*db* mice. Notably, *Elovl6* deficiency has been shown to improve glycemic control in *db*/*db* mice. In humans, *Elovl6* has been implicated in the development and progression of MASH by contributing to increased hepatic oxidative stress, inflammation and fibrosis.	(34,35)
Ephb2	Downregulated	The *Ephb2* gene encodes EphB2, a member of the Eph receptor family of transmembrane receptor tyrosine kinases that serves a key role in cell-cell signaling, often through interaction with ephrin-B ligands. EphB2 has been implicated in promoting inflammation and fibrosis in MASH. Specifically, increased expression of *Ephb2* in liver tissue is associated with exacerbated fibrosis, and studies in preclinical models have shown that *Ephb2* deficiency attenuates liver fibrosis and inflammation.	(36,37)
Cidea	Downregulated	The *Cidea* gene encodes the protein CIDEA, which serves a notable role in various metabolic processes, particularly in the regulation of lipid droplet formation and energy homeostasis. CIDEA functions as a sensor for dietary saturated fatty acids and is a known transcriptional target of sterol regulatory element-binding protein 1. Consistent with its role in lipid metabolism, *Cidea* expression is markedly elevated in the livers of obese mice and humans. The hepatic overexpression of *Cidea* increases lipid accumulation and promotes the formation of larger lipid droplets. Conversely, *Cidea* knockout in mice reduces these lipid abnormalities, highlighting its key role in regulating hepatic lipid metabolism.	(38,39)
Me1	Downregulated	The *Me1* gene encodes malic enzyme 1, a cytosolic enzyme that catalyzes the oxidative decarboxylation of malate to pyruvate, concomitantly generating NADPH. This enzyme serves a key role in linking glycolysis and the citric acid cycle, and the NADPH produced is essential for various anabolic pathways, including *de novo* fatty acid and cholesterol biosynthesis. Consistent with its role in lipogenesis, studies in mice have demonstrated that *Me1* knockdown can notably reduce adiposity and hepatic steatosis in obese models.	(40,41)
Arrdc3	Downregulated	The *Arrdc3* gene encodes ARRD3, a member of the arrestin family of proteins that regulate various cellular processes, including protein trafficking and G-protein-coupled receptor signaling. ARRD3 has been shown to directly interact with SCD1, a key enzyme in monounsaturated fatty acid synthesis. This interaction stabilizes SCD1 protein levels, thereby promoting increased lipid production and accumulation. In mice, liver-specific deletion of *Arrdc3* markedly increases insulin sensitivity, while whole-body *Arrdc3* knockout mice exhibit resistance to the metabolic complications of obesity, including reduced adiposity and hepatic steatosis.	(42,43)
Fasn	Downregulated	The *Fasn* gene encodes fatty acid synthase, a key enzyme in *de novo* lipogenesis that catalyzes the synthesis of long-chain fatty acids from ACC and malonyl-CoA. Consistent with its central role in lipid synthesis, hepatic expression of *Fasn* is increased in both mouse and human livers affected by steatosis. Furthermore, pharmacological inhibition of *Fasn* has demonstrated efficacy in ameliorating steatosis in mouse models and in human patients with MASLD.	(44,45)

Table II. Continued.

Gene	Effect of SR4	Gene function and association	(Refs.)
Acaca	Downregulated	The *Acaca* gene encodes ACC1, a crucial enzyme in fatty acid biosynthesis. ACC1 catalyzes the rate-limiting step in the conversion of ACC to malonyl-CoA, which serves as a key precursor for long-chain fatty acid synthesis. Consistent with its notable role in lipogenesis, hepatic overexpression of *Acaca* is associated with increased fat accumulation and can contribute to MASLD. Importantly, pharmacological inhibition of ACC1 has been shown to reduce hepatic steatosis and improve insulin sensitivity in both mice and humans.	(46,47)
Cyp3a41a	Upregulated	The *Cyp3a41a* gene encodes the cytochrome P450 enzyme 3A41. CYP3A enzymes, including *Cyp3a41a*, are known for their broad substrate specificity, metabolizing a vast array of endogenous compounds such as steroid hormones, bile acids and cholesterol, thereby contributing to their regulation and systemic homeostasis. The related isoform CYP3A4 is reduced in animals and individuals with MASLD and MASH.	(48,49)
Cyp4a12b	Upregulated	In mice, *Cyp4a12b* encodes a cytochrome P450 ω-hydroxylase involved in the metabolism of fatty acids and their oxygenated derivatives (oxylipins). It catalyzes the ω-hydroxylation of arachidonic acid, forming 20-hydroxyeicosatetraenoic acid. *Cyp4a12b* expression is reduced during the development of liver fibrosis and inflammation.	(50,51)
Mt1	Upregulated	Hepatic expression of *Mt1*, a gene encoding metallothionein 1, is markedly downregulated in liver tissues of patients with MASH and in high-fat diet-induced mouse models. This hepatic downregulation of *Mt1* is associated with increased TG and total cholesterol levels, exacerbated lipid accumulation, and elevated liver fibrosis and inflammation	(52,53)

ARRD3, arrestin domain containing 3; CIDEA, cell death-inducing DFF45-like effector A; MASLD, metabolic dysfunction-associated steatotic liver disease; MASH, metabolic dysfunction-associated steatohepatitis; NADPH, nicotinamide adenine dinucleotide phosphate (reduced form); SCD1, stearoyl-CoA desaturase 1.

the STRING database with a high-confidence interaction score threshold of 0.7. The resulting network, derived from the 642 DEGs, comprised 328 nodes (representing 328 of the DEGs) and 764 edges, forming its largest connected component (Fig. 7A). This number of observed edges was significantly greater than expected for a random network of similar size ($P \leq 1x10^{-16}$), indicating that the encoded proteins are more interconnected than would occur by chance and are likely involved in biologically related processes. Among the 328 genes in the network, 118 were upregulated and 210 were downregulated. Network clustering analysis using the 'MCODE' plugin in Cytoscape identified ≥20 subnetwork modules. The top five modules were functionally enriched in distinct metabolic processes. Cluster 1 was associated with steroid hormone biosynthesis and retinol metabolism, cluster 2 with the pentose phosphate pathway (PPP) and glycolysis, cluster 3 with fatty acid synthesis and pyruvate metabolism, cluster 4 with lipid droplet metabolism and cluster 5 with cellular amino acid catabolic pathways (Fig. 7B-F).

Due to the central role of AMPK in regulating nutrient and energy metabolism, along with its increased protein phosphorylation and pathway enrichment in the present study, a focused PPI subnetwork was constructed to explore functionally connected gene modules. This subnetwork encompassed DEGs implicated in AMPK signaling, amino acid metabolism, lipid metabolism and glucose metabolism, including key components of the PPP and pyruvate metabolism, as identified through GO and KEGG enrichment analyses. The resulting network comprised 65 nodes and 191 edges, underscoring a high degree of interconnectivity among genes involved in core metabolic processes (Fig. 7G). Notably, multiple interactions within the subnetwork converged on key AMPK regulatory nodes, including *Acaca* and *Acacb* (encoding ACC 1 and 2, respectively), *Pparg* (PPARγ) and mammalian target of rapamycin (*mTor*), highlighting the intricate integration of lipid biosynthesis with energy-sensing pathways. To pinpoint central regulatory elements within the subnetwork, hub gene analysis was performed using the MCC algorithm within the 'cytoHubba' plugin. This analysis identified a number

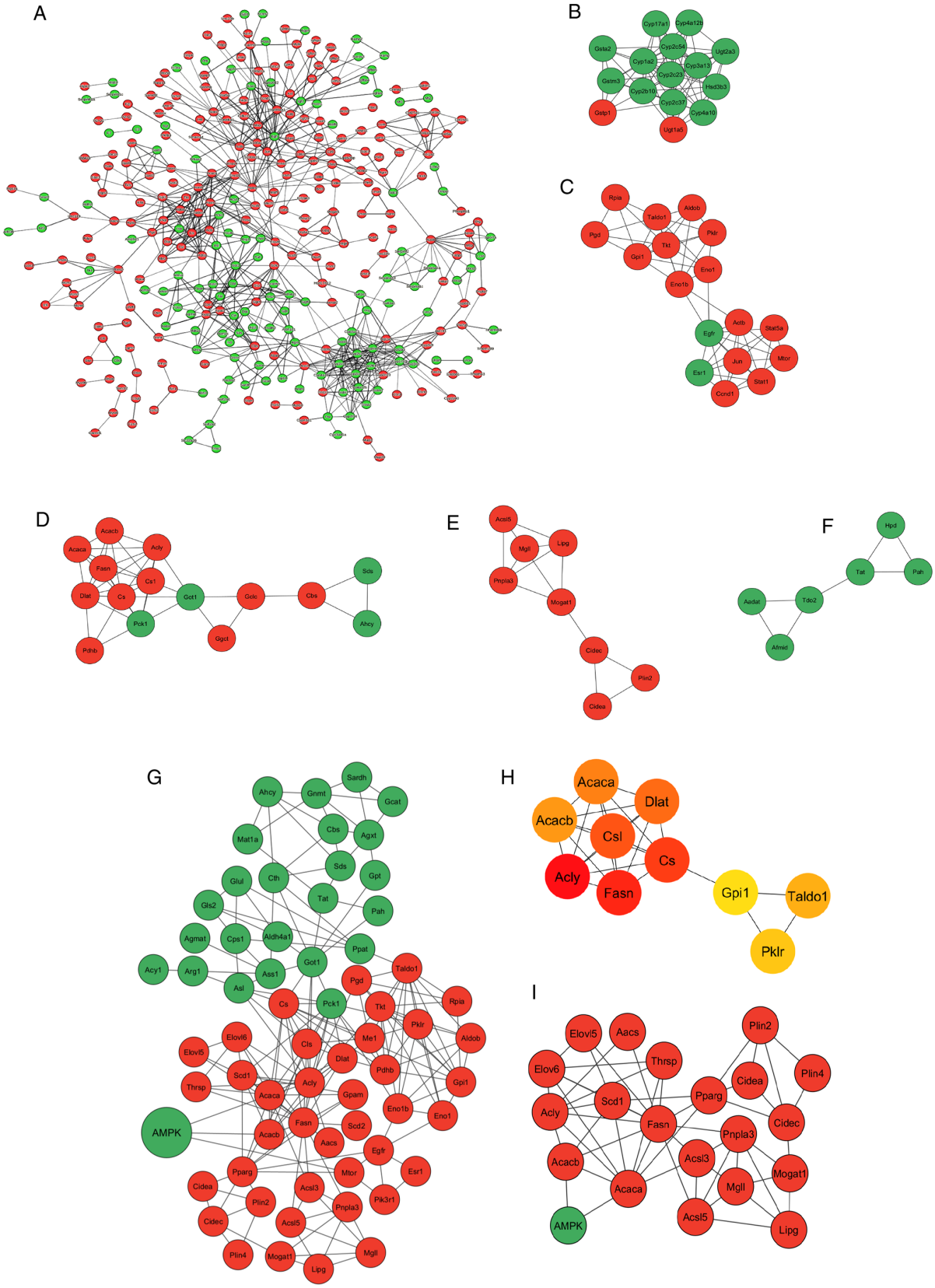

Figure 7. PPI networks and subnetworks (modules) of DEGs in SR4-treated *db/db* mice livers. (A) PPI network of all 642 DEGs. For clarity, disconnected nodes are not shown. Circles represent genes (nodes) and lines between them represent interactions (edges). The top 5 most significant modules from the PPI network of DEGs, identified by MCODE screening. These modules are associated with (B) steroid hormone biosynthesis, (C) pentose phosphate pathway and glycolysis, (D) fatty acid synthesis and pyruvate metabolism, (E) lipid droplet metabolism and (F) metabolism of amino acids and derivatives. (G) PPI subnetwork for genes associated with AMPK and nutrient and energy metabolic pathways, as identified by GO and KEGG enrichment analyses. (H) Top 10 hub genes identified in the subnetwork in (G) using the 'Maximal Clique Centrality' plugin of CytoHubba. (I) Putative AMPK/PPARγ-associated regulatory axis for fatty acid and TG synthesis, TG production, lipid droplet formation and storage. In panels (A-G) and (I), green and red circles represent upregulated and downregulated genes, respectively. In panel (H), red circles indicate hub genes with high-ranking scores, while yellow rectangles represent hub genes with lower-ranking scores. PPARγ, peroxisome proliferator-activated receptor γ; PPI, protein-protein interaction; TG, triglycerides; DEGs, differentially expressed genes.

of prominent hub genes, with *Fasn* and *Acly* exhibiting the highest MCC scores (Fig. 7H). Additionally, a putative AMPK/PPARγ-associated regulatory network was identified, linking fatty acid synthesis, TG production, lipid droplet formation and storage (Fig. 7I). Collectively, these findings suggested that genes involved in lipid metabolism serve key roles in mediating the SR4-induced metabolic reprogramming in the liver.

Discussion

Mitochondrial uncouplers have emerged as a promising class of therapeutics for metabolic disorders such as obesity, T2D, MASLD and certain cancer types. These compounds act by dissipating the proton gradient across the mitochondrial inner membrane. By uncoupling oxidative phosphorylation from ATP synthesis, they increase energy expenditure and improve metabolic parameters, making them promising candidates for treating diseases characterized by nutrient excess and metabolic dysfunction (9-11,17). Numerous uncouplers have demonstrated both metabolic efficacy and favorable safety profiles in preclinical models and are now advancing through clinical development. Niclosamide, originally developed as an antihelmintic agent, exhibits mitochondrial uncoupling properties and is currently under clinical evaluation for cancer therapy (trial no. NCT02519582 and NCT05188170) with additional metabolic benefits reported in a preclinical study (54). Other uncouplers such as TLC-6740, under investigation for obesity and T2D (trial no. NCT05822544) and HU6, which is in phase II trials for MASH (trial no. NCT04874233 and NCT05979779), highlight the increasing clinical momentum for this therapeutic strategy.

SR4 represents a newer class of mitochondrial uncouplers known as synthetic anion fatty acid transporters (15,16). These compounds facilitate the transport of fatty acid anions across the mitochondrial inner membrane, where the anions act as proton shuttles to induce controlled mitochondrial uncoupling. Unlike classical protonophores such as FCCP and 2,4-dinitrophenol which cause rapid and complete collapse of the mitochondrial membrane potential, leading to full depolarization, severe off-target effects including plasma membrane disruption and dose-dependent cytotoxicity (55), fatty acid anion transporters such as SR4 may provide greater mitochondrial specificity and safety through gradual, physiologically controlled depolarization. This mechanism of action renders SR4 particularly promising for long-term treatment of chronic metabolic conditions such as obesity, T2D and MASH, where sustained and safe increase in energy expenditure and metabolism is therapeutically advantageous.

Previous studies have shown that a BW loss of 5-10% is sufficient to markedly improve insulin sensitivity, lipid profiles and hepatic steatosis, thereby lowering the risk for T2D and MASLD (56,57). In the present study, SR4 treatment led to a significant 13% reduction in BW in *db/db* mice across 5 weeks. This weight loss occurred without any decrease in food intake, indicating that SR4 primarily enhances metabolism and energy expenditure rather than suppressing appetite. Notably, this weight reduction was associated with a favorable shift in body composition as SR4 specifically reduced fat mass while preserving lean mass. This outcome is clinically desirable as numerous existing weight loss drugs such as glucagon-like peptide-1 receptor (GLP-1R) agonists and dual GLP-1R/glucose-dependent insulinotropic polypeptide receptor agonists, can cause a loss of both fat and lean tissue mass (58). Preserving lean mass during weight loss reduction is key for maintaining muscle strength and healthy metabolism and decreasing risk of physical injury (59).

In the present study, SR4 treatment improved hyperglycemia and dyslipidemia and exerted potent anti-steatotic effects in *db/db* mice, as evidenced by reduced liver weight, lower TG content and fewer hepatic lipid droplets. Mechanistically, SR4 increased the hepatic AMP:ATP ratio, leading to activation of AMPK, a central regulator of energy homeostasis that promotes catabolic pathways while inhibiting anabolic processes such as *de novo* lipogenesis (60). Transcriptomic and qPCR analyses revealed that SR4 suppressed several key lipogenic genes and transcription factors, including *Acaca*, *Acly*, *Fasn*, *Scd1*, *Cebpa*, *Srebf1* and *Pparg*. with additional enrichment analyses confirming downregulation of fatty acid biosynthesis and lipid storage pathways. PPI networks identified gene clusters downstream of AMPK and PPARγ signaling, implicating a coordinated regulatory axis controlling fatty acid synthesis, TG accumulation and lipid droplet formation. These results are consistent with previous observations in HFD-fed obese mice (17) and align with previous studies linking AMPK-dependent pathways involving *Acaca*, *Fasn*, *Scd1*, *Elovl6* and *Mogat1* as key mediators of *de novo* lipid synthesis (61). SR4 has also been shown to prevent hepatic steatosis, fibrosis and liver injury in TERF2 interacting protein-deficient MASH mice through AMPK activation (62). Thus, SR4 appears to improve hepatic metabolic homeostasis by activating AMPK and reprogramming lipid metabolism.

Both qPCR and transcriptomic analyses also revealed that SR4 downregulated hepatic PPARγ expression. While PPARγ is predominantly expressed in adipose tissue, the ectopic induction of PPARγ is observed in the steatotic liver. Genetic deletion or pharmacological inhibition of hepatic PPARγ reduces steatosis and inflammation (63,64). Furthermore, PPARγ activity is negatively regulated by AMPK and mTOR, with AMPK phosphorylation suppressing its transcriptional activity and mTOR inhibition attenuating lipogenesis (65,66). Consistent with this, SR4 activated AMPK and inhibited mTOR, providing a plausible mechanism for reduced PPARγ expression and subsequent improvement in hepatic lipid metabolism.

Mitochondrial respiratory dysfunction is a hallmark of metabolic diseases. A decrease in mitochondrial respiration has been observed in obese T2D mice (67). Using Seahorse extracellular flux analyses, the present study found that SR4 significantly enhanced mitochondrial respiration, increasing OCR across multiple respiratory states including basal (state 2), ADP-stimulated (state 3), uncoupled maximal respiration (state 3u), proton leak and SRC. This improved respiratory capacity suggests that SR4 helps to improve the use of metabolic substrates for energy by the liver, contributing to increased whole-body energy expenditure. Similar effects have been observed with the mitochondrial uncoupler BAM15, which enhances mitochondrial oxidative capacity partly by peroxisome proliferator-activated receptor γ coactivator-1 α activation (68). Whether SR4 promotes

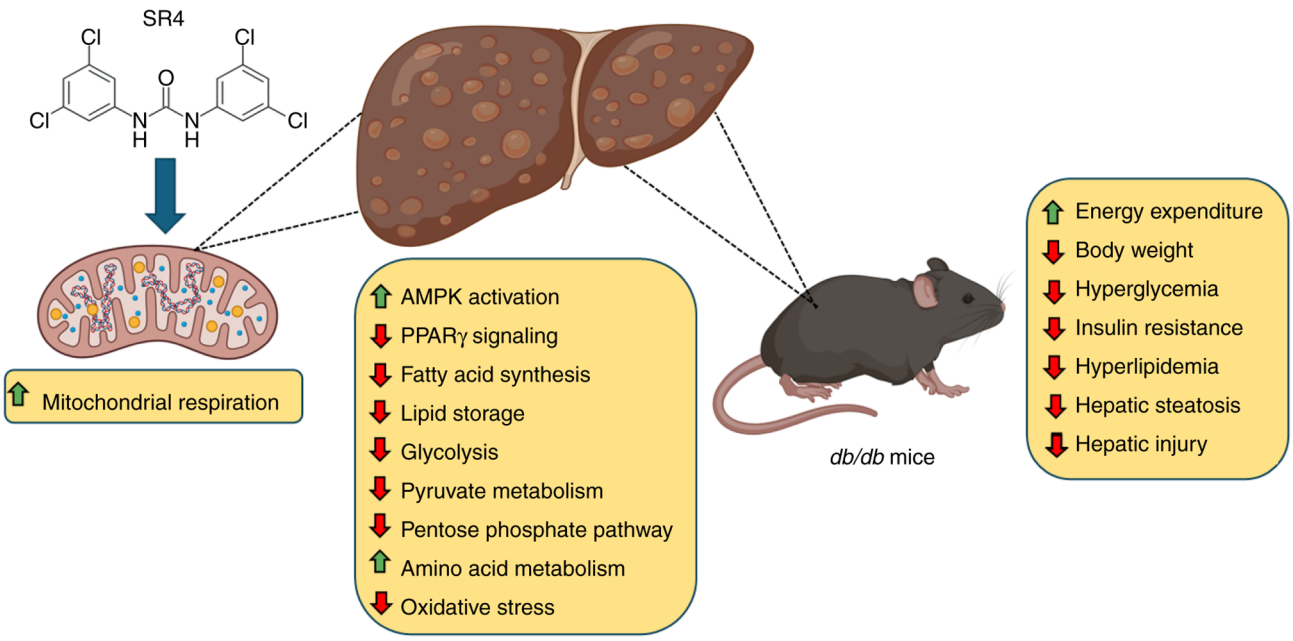

Figure 8. Summary of the metabolic effects of SR4 on the liver of *db/db* mice. SR4 functions as a mitochondrial uncoupler by facilitating fatty acid-activated proton transport across the inner mitochondrial membrane. As a bisaryl urea-based anion transporter, SR4 enhances the flip-flop movement of deprotonated fatty acids across the inner mitochondrial membrane, promoting proton leak. This uncoupling disrupts the mitochondrial proton gradient, leading to reduced ATP synthesis. The resulting decline in cellular ATP levels activates AMPK, a key regulator of energy homeostasis. In the liver, AMPK activation suppresses lipogenic pathways, including PPARγ signaling, while promoting catabolic processes that support mitochondrial function and energy utilization. This metabolic reprogramming enhances mitochondrial respiration and oxidative capacity, reduces oxidative stress and improves metabolic flexibility. Collectively, these effects contribute to broad metabolic improvements in *db/db* mice, including increased energy expenditure and metabolic activity, reduced nody weight, improved glycemic control, enhanced insulin sensitivity, correction of dyslipidemia and attenuation of hepatic steatosis and injury. Figure partly created in BioRender. PPARγ, peroxisome proliferator-activated receptor γ.

mitochondrial biogenesis through similar pathways remains to be investigated.

SR4 also modulated oxidative stress, a key contributor to liver injury in metabolic disease. The present study found that SR4 treatment significantly reduced hepatic MDA levels, indicating attenuation of lipid peroxidation. This effect was accompanied by increased activity of GSH-linked antioxidant enzymes, including GPx and GST. These enzymes serve key roles in detoxifying reactive oxygen species as GPx reduces hydrogen peroxide and lipid hydroperoxides using reduced GSH, while GSTs catalyze the conjugation of GSH to electrophilic substrates, facilitating their excretion. Transcriptomic analysis further supported this observation, revealing significant upregulation of genes involved in GSH metabolism, such as GSH S-transferase α 2, GSH S-transferase κ 1, GSH S-transferase mu 7 and GSH S-transferase θ 3. This dual action, enhancing mitochondrial respiratory function while bolstering antioxidant defenses, could be an important mechanism by which SR4 prevents liver injury in *db/db* mice.

Beyond lipid metabolism, transcriptomic analysis also revealed that SR4 induces a broader metabolic reprogramming in the liver of *db/db mice*. SR4 upregulated genes involved in 'Amino acid metabolic process', while downregulating those associated with 'Glycolysis/Gluconeogenesis', 'Pyruvate metabolism' and the 'PPP'. This shift resembles the adaptive metabolic response observed during caloric restriction or fasting, where anabolic pathways are suppressed and catabolic processes are enhanced to maintain energy homeostasis and preserve mitochondrial function under nutrient-limited conditions. A key feature of this adaptive response is the enhancement of glutamine metabolism. Through glutaminolysis, glutamine contributes to anaplerosis by replenishing TCA cycle intermediates, thereby supporting mitochondrial ATP production when glycolytic flux is reduced (69). Glutamine also serves as a precursor for GSH synthesis, thereby enhancing cellular antioxidant defenses (70). These functions are especially important under conditions of energetic stress, where metabolic flexibility is vital for cellular survival and function. Additionally, during amino acid catabolism, the removal and transfer of the amino group through deamination and transamination provides carbon skeletons that can be utilized in the TCA cycle for energy generation, while the α-amino nitrogen atoms are converted into ammonia, which is then detoxified and converted to urea through the urea cycle for safe excretion (71). Notably, SR4 increased the expression of urea cycle genes, reflecting greater amino acid turnover and nitrogen disposal.

The downregulation of the PPP in liver of SR4-treated mice further underscores a redirection of glucose flux away from anabolic biosynthesis. As a major source of NADPH, the PPP primarily supports reductive biosynthesis and maintains redox balance through the regeneration of reduced GSH (72). Suppression of this pathway may therefore indicate a systemic reduction in overall biosynthetic activity, aligning with the energy-conserving, catabolic state induced by SR4. Additionally, inhibition of pyruvate metabolism may restrict the production of ACC, a central metabolic intermediate required for both TCA cycle activity and *de novo* lipogenesis. Limiting ACC availability could contribute to the observed suppression of lipogenic gene expression and the reduction

in hepatic TG content seen with SR4 treatment. Collectively, these findings suggest that SR4 promotes a hepatic metabolic program reminiscent of nutrient deprivation, characterized by metabolic flexibility, enhanced oxidative metabolism and inhibition of lipogenesis, which may underlie its therapeutic benefits in obesity, insulin resistance and MASLD.

Despite these promising findings, the present study has some limitations. First, only male *db*/*db* mice were used, which may not capture sex-dependent metabolic responses, as female mice often exhibit different disease progression and therapeutic sensitivity (73). Future studies should include both sexes to enhance translational relevance. Second, the absence of comparisons with standard anti-diabetic or anti-steatosis drugs limits direct clinical interpretation. Notably, a recent head-to-head study of female *db*/*db* mice compared the mitochondria uncoupler BAM15 with semaglutide, rosiglitazone and niclosamide and reported that BAM15 exhibited greater weight loss reduction and improvements in dyslipidemia and steatosis (74). Third, the present investigation focused solely on hepatic outcomes, leaving the systemic impact of SR4 on other metabolically active tissues such as skeletal muscles and adipose tissues to be determined. Finally, the absence of pharmacokinetic and bioavailability studies limits the understanding of SR4 *in vivo*. Our preliminary study has shown that SR4 preferentially accumulates in adipose tissues and liver, consistent with its high lipophilic properties. Future work will need to address these gaps to fully elucidate the therapeutic potential and mechanism of action of SR4.

In conclusion, the present study provided evidence that SR4 is an effective orally administered agent that ameliorates multiple hallmark features of metabolic dysfunction in T2D, including hyperglycemia, insulin resistance, dyslipidemia, hepatic steatosis and liver injury. SR4 promoted BW loss and improved body composition by reducing fat mass while preserving lean mass, without suppressing appetite, which highlighted its potential as a safe and sustainable therapeutic strategy. Mechanistically, these effects appeared to be mediated through mitochondrial uncoupling, AMPK activation, modulation of mTOR and PPARγ signaling, improved mitochondrial bioenergetics, antioxidant defense and global metabolic reprogramming (Fig. 8). Together, these findings support further preclinical and clinical development of SR4 and related fatty acid anion transporters as a novel therapeutic class for treating metabolic diseases.

Acknowledgements

The authors wish to thank Dr Patrick Fueger (Comprehensive Metabolic Phenotyping Core Facility) for assistance in the indirect calorimetry studies, Dr Lu Yang and Dr Xiwei Wu (Integrative Genomics and Bioinformatics Core) and Dr Yate-Ching Yuan (Division of Research Informatics) for the help in RNA sequencing data analyses and database submission, and Mrs. Leslie Smith-Powell for the nucleotide measurements (Analytical Pharmacology Core).

Funding

The present study was partly supported by the Samuel Rahbar Diabetes and Drug Discovery Endowment, Arthur Riggs Diabetes & Metabolism Research Institute and innovation grant from the Wanek Family Project for Type 1 Diabetes at City of Hope.

Availability of data and materials

The data generated in the present study may be found in the National Center for Biotechnology Information Gene Expression Omnibus database under accession number GSE308701 or at the following URL: https://www.ncbi.nlm.nih.gov/geo/query/acc.cgi?acc=GSE308701.

Authors' contributions

JLF conceptualized, designed and conducted the experiments, collected and analyzed data and wrote the manuscript. SS conducted experiments, collected data and analyzed results and reviewed the manuscript. JS performed experiments, collected data and reviewed the manuscript. All authors confirm the authenticity of all the raw data. All authors read and approved the final version of the manuscript.

Ethics approval and consent to participate

All animal experiments performed in the present study were approved by the Institutional Animal Care and Use Committee of the City of Hope National Medical Center (approval no. 12004; Duarte, USA).

Patient consent for publication

Not applicable.

Competing interests

The authors declare that they have no competing interests.

Use of artificial intelligence tools

During the preparation of this work, artificial intelligence tools were used to improve the readability and language of the manuscript or to generate images, and subsequently, the authors revised and edited the content produced by the artificial intelligence tools as necessary, taking full responsibility for the ultimate content of the present manuscript.

References

1. American Diabetes Association Professional Practice Committee: Classification and diagnosis of diabetes: 2. Diagnosis and Classification of Diabetes: Standards of Care in Diabetes-2024. Diabetes Care 47 (Suppl 1): S20-S42 2024.
2. International Diabetes Federation: IDF Diabetes Atlas, 11th edition. Brussels, Belgium, IDF, 2025.
3. Khan MAB, *et al*: Global burden of diabetes and its projections to 2050: A systematic review. Lancet Diabetes Endocrinol, 2023.
4. Mooradian AD: Dyslipidemia in type 2 diabetes mellitus. Nat Clin Pract Endocrinol Metab 5: 150-159, 2009.
5. Caturano A, D'Angelo M, Mormone A, Russo V, Mollica MP, Salvatore T, Galiero R, Rinaldi L, Vetrano E, Marfella R, *et al*: Oxidative stress in type 2 diabetes: Impacts from pathogenesis to lifestyle modifications. Curr Issues Mol Biol 45: 6651-6666, 2023.

6. Younossi ZM, Golabi P, Price JK, Owrangi S, Gundu-Rao N, Satchi R and Paik JM: The global epidemiology of nonalcoholic fatty liver disease and nonalcoholic steatohepatitis among patients with type 2 diabetes. Clin Gastroenterol Hepatol 22: 1999-2010.e8 2024.
7. Younossi ZM, Kalligeros M and Henry L: Epidemiology of metabolic dysfunction-associated steatotic liver disease. Clin Mol Hepatol 31 (Suppl): S32-S50, 2025.
8. Davies MJ, Aroda VR, Collins BS, Gabbay RA, Green J, Maruthur NM, Rosas SE, Del Prato S, Mathieu C, Mingrone G, *et al*: Management of hyperglycemia in type 2 diabetes, 2022. A consensus report by the American diabetes association (ADA) and the european association for the study of diabetes (EASD). Diabetes Care 45: 2753-2786, 2022.
9. Goedeke L and Shulman GI: Therapeutic potential of mitochondrial uncouplers for the treatment of metabolic associated fatty liver disease and NASH. Mol Metab 46: 101178, 2021.
10. Alexopoulos SJ, Chen SY, Brandon AE, Salamoun JM, Byrne FL, Garcia CJ, Beretta M, Olzomer EM, Shah DP, Philp AM, *et al*: Mitochondrial uncoupler BAM15 reverses diet-induced obesity and insulin resistance in mice. Nat Commun 11: 2397, 2020.
11. Kanemoto N, Okamoto T, Tanabe K, Shimada T, Minoshima H, Hidoh Y, Aoyama M, Ban T, Kobayashi Y, Ando H, *et al*: Antidiabetic and cardiovascular beneficial effects of a liver-localized mitochondrial uncoupler. Nat Commun 10: 2172, 2019.
12. Figarola JL, Singhal J, Tompkins JD, Rogers GW, Warden C, Horne D, Riggs AD, Awasthi S and Singhal SS: SR4 Uncouples mitochondrial oxidative phosphorylation, modulates AMP-dependent kinase (AMPK)-mammalian target of rapamycin (mTOR) signaling, and inhibits proliferation of HepG2 hepatocarcinoma cells. J Biol Chem 290: 30321-30341, 2015.
13. Singhal SS, Figarola J, Singhal J, Nagaprashantha L, Berz D, Rahbar S and Awasthi S: Novel compound 1,3-bis (3,5-dichlorophenyl) urea inhibits lung cancer progression. Biochem Pharmacol 86: 1664-1672, 2013.
14. Figarola JL, Singhal J, Singhal S, Kusari J and Riggs A: Bioenergetic modulation with the mitochondria uncouplers SR4 and niclosamide prevents proliferation and growth of treatment-naïve and vemurafenib-resistant melanomas. Oncotarget 9: 36945-36965, 2018.
15. Rawling T, MacDermott-Opeskin H, Roseblade A, Pazderka C, Clarke C, Bourget K, Wu X, Lewis W, Noble B, Gale PA, *et al*: Aryl urea substituted fatty acids: A new class of protonophoric mitochondrial uncoupler that utilises a synthetic anion transporter. Chem Sci 11: 12677-12685, 2020.
16. York E, McNaughton DA, Roseblade A, Cranfield CG, Gale PA and Rawling T: Structure-activity relationship and mechanistic studies of bisaryl urea anticancer agents indicate mitochondrial uncoupling by a fatty Acid-Activated Mechanism. ACS Chem Biol 17: 2065-2073, 2022.
17. Figarola JL, Singhal P, Rahbar S, Gugiu BG, Awasthi S and Singhal SS: COH-SR4 reduces body weight, improves glycemic control and prevents hepatic steatosis in high fat diet-induced obese mice. PLoS One 8: e83801, 2013.
18. Lau JK, Zhang X and Yu J: Animal models of non-alcoholic fatty liver disease: Current perspectives and recent advances. J Pathol 241: 36-44, 2017.
19. Benedé-Ubieto R, Estévez-Vázquez O, Ramadori P, Cubero FJ and Nevzorova YA: Guidelines and considerations for metabolic tolerance tests in mice. Diabetes Metab Syndr Obes 13: 439-450, 2020.
20. Noeman SA, Hamooda HE and Baalash AA: Biochemical study of oxidative stress markers in the liver, kidney and heart of high fat diet induced obesity in rats. Diabetol Metab Syndr 3: 17, 2011.
21. Fraga CG, Leibovitz BE and Tappel AL: Lipid peroxidation measured as thiobarbituric acid-reactive substances in tissue slices: Characterization and comparison with homogenates and microsomes. Free Radic Biol Med 4: 155-1561, 1988.
22. Iuso A, Repp B, Biagosch C, Terrile C and Prokisch H: Assessing mitochondrial bioenergetics in isolated mitochondria from various mouse tissues using Seahorse XF96 analyzer. Methods Mol Biol 1567: 217-230, 2017.
23. Livak KJ and Schmittgen TD: Analysis of relative gene expression data using real-time quantitative PCR and the 2(-delta delta C(T)) method. Methods 25: 402-408, 2001.
24. Robinson MD, McCarthy DJ and Smyth GK: edgeR: A Bioconductor package for differential expression analysis of digital gene expression data. Bioinformatics 26: 139-140, 2010.
25. Love MI, Huber W and Anders S: Moderated estimation of fold change and dispersion for RNA-seq data with DESeq2. Genome Biol 15: 550, 2014.
26. Goedhart J and Luijsterburg MS: VolcaNoseR is a web app for creating, exploring, labeling and sharing volcano plots. Sci Rep 10: 20560, 2020.
27. Huang DW, Sherman BT, Lempicki RA and Lemoine S: DAVID: A web server for functional enrichment analysis and functional annotation of gene lists (2021 update). Nucleic Acids Res 50: W216-W221, 2022.
28. Szklarczyk D, Nastou K, Koutrouli M, Kirsch R, Mehryary F, Hachilif R, Hu D, Peluso ME, Huang Q, Fang T, *et al*: The STRING database in 2025: Protein networks with directionality of regulation. Nucleic Acids Res 53: D730-D737, 2025.
29. Shannon P, Markiel A, Ozier O, Baliga NS, Wang JT, Ramage D, Amin N, Schwikowski B and Ideker T: Cytoscape: A software environment for integrated models of biomolecular interaction networks. Genome Res 13: 2498-2504, 2003.
30. Bader GD and Hogue CW: An automated method for finding molecular complexes in large protein interaction networks. BMC Bioinformatics 4: 2, 2003.
31. Chin CH, Chen SH, Wu HH, Ho CW, Ko MT and Lin CY: cytoHubba: Identifying hub objects and sub-networks from complex interactome. BMC Syst Biol 8 (Suppl 4): S11, 2014.
32. Burke SJ, Batdorf HM, Burk DH, Noland RC, Eder AE, Boulos MS, Karlstad MD and Collier JJ: Db/db mice exhibit features of human type 2 diabetes that are not present in weight-matched C57BL/6J mice fed a Western diet. J Diabetes Res 2017: 8503754, 2017.
33. Sahai A, Malladi P, Pan X, Paul R, Melin-Aldana H, Green RM and Whitington PF: Obese and diabetic db/db mice develop marked liver fibrosis in a model of nonalcoholic steatohepatitis: Role of short-form leptin receptors and osteopontin. Am J Physiol Gastrointest Liver Physiol 287: G1035-G1043, 2004.
34. Zhao H, Matsuzaka T, Nakano Y, Motomura K, Tang N, Yokoo T, Okajima Y, Han SI, Takeuchi Y, Aita Y, *et al*: Elovl6 deficiency improves glycemic control in diabetic db/db mice by expanding β-Cell mass and increasing insulin secretory capacity. Diabetes 66:1833-1846, 2017.
35. Matsuzaka T, Atsumi A, Matsumori R, Nie T, Shinozaki H, Suzuki-Kemuriyama N, Kuba M, Nakagawa Y, Ishii K, Shimada M, *et al*: Elovl6 promotes nonalcoholic steatohepatitis. Hepatology 56: 2199-2208, 2012.
36. Xiao Y, Batmanov K, Hu W, Zhu K, Tom AY, Guan D, Jiang C, Cheng L, McCright SJ, Yang EC, *et al*: Hepatocytes demarcated by EphB2 contribute to the progression of nonalcoholic steatohepatitis. Sci Transl Med 15: eadc9653, 2023.
37. Mimche PN, Lee CM, Mimche SM, Thapa M, Grakoui A, Henkemeyer M and Lamb TJ: EphB2 receptor tyrosine kinase promotes hepatic fibrogenesis in mice via activation of hepatic stellate cells. Sci Rep 8: 2532, 2018.
38. Zhou L, Xu L, Ye J, Li D, Wang W, Li X, Wu L, Wang H, Guan F and Li P: Cidea promotes hepatic steatosis by sensing dietary fatty acids. Hepatology 56: 95-107, 2012.
39. Sans A, Bonnafous S, Rousseau D, Patouraux S, Canivet CM, Leclere PS, Tran-Van-Nhieu J, Luci C, Bailly-Maitre B, Xu X, *et al*: The differential expression of Cide family members is associated with NAFLD progression from steatosis to steatohepatitis. Sci Rep 9: 7501, 2019.
40. Simmen FA, Pabona JMP, Al-Dwairi A, Alhallak I, Montales MTE and Simmen RCM: Malic enzyme 1 (ME1) promotes adiposity and hepatic steatosis and induces circulating insulin and leptin in obese female mice. Int J Mol Sci 24: 6613, 2023.
41. Al-Dwairi A, Pabona JM, Simmen RC and Simmen FA: Cytosolic malic enzyme 1 (ME1) mediates high fat diet-induced adiposity, endocrine profile, and gastrointestinal tract proliferation-associated biomarkers in male mice. PLoS One 7: e46716, 2012.
42. Batista TM, Dagdeviren S, Carroll SH, Cai W, Melnik VY, Noh HL, Saengnipanthkul S, Kim JK, Kahn CR and Lee RT: Arrestin domain-containing 3 (Arrdc3) modulates insulin action and glucose metabolism in liver. Proc Natl Acad Sci USA 117: 6733-6740, 2020.
43. Patwari P, Emilsson V, Schadt EE, Chutkow WA, Lee S, Marsili A, Zhang Y, Dobrin R, Cohen DE, Larsen PR, *et al*: The arrestin domain-containing 3 protein regulates body mass and energy expenditure. Cell Metab 14: 671-683, 2011.
44. Dorn C, Riener MO, Kirovski G, Saugspier M, Steib K, Weiss TS, Gäbele E, Kristiansen G, Hartmann A and Hellerbrand C: Expression of fatty acid synthase in nonalcoholic fatty liver disease. Int J Clin Exp Pathol 3: 505-514, 2010.

45. O'Farrell M, Duke G, Crowley R, Buckley D, Martins EB, Bhattacharya D, Friedman SL and Kemble G: FASN inhibition targets multiple drivers of NASH by reducing steatosis, inflammation and fibrosis in preclinical models. Sci Rep 12: 15661, 2022.
46. Mateo-Marín MA and Alves-Bezerra M: Targeting acetyl-CoA carboxylases for the treatment of MASLD. J Lipid Res 65: 100676, 2024.
47. Tamura YO, Sugama J, Iwasaki S, Sasaki M, Yasuno H, Aoyama K, Watanabe M, Erion DM and Yashiro H: Selective Acetyl-CoA carboxylase 1 inhibitor improves hepatic steatosis and hepatic fibrosis in a preclinical nonalcoholic steatohepatitis model. J Pharmacol Exp Ther 379: 280-289, 2021.
48. Jamwal R, de la Monte SM, Ogasawara K, Adusumalli S, Barlock BB and Akhlaghi F: Nonalcoholic fatty liver disease and diabetes are associated with decreased CYP3A4 protein expression and activity in human liver. Mol Pharm 15: 2621-2632, 2018.
49. Woolsey SJ, Mansell SE, Kim RB, Tirona RG and Beaton MD: CYP3A activity and expression in nonalcoholic fatty liver disease. Drug Metab Dispos 43: 1484-1490, 2015.
50. Ping DB, Sun X, Peng Y and Liu CH: Cyp4a12-mediated retinol metabolism in stellate cells is the antihepatic fibrosis mechanism of the Chinese medicine Fuzheng Huayu recipe. Chin Med 18: 51, 2023.
51. Theken KN, Deng Y, Kannon MA, Miller TM, Poloyac SM and Lee CR: Activation of the acute inflammatory response alters cytochrome P450 expression and eicosanoid metabolism. Drug Metab Dispos 39: 22-29, 2011.
52. Li X, Zhong S, Sun Y, Huang X, Li Y, Wang L, Wu Y, Yang M, Yuan HX, Liu J and Zang S: Integration analysis identifies the role of metallothionein in the progression from hepatic steatosis to steatohepatitis. Front Endocrinol (Lausanne) 13: 951093, 2022.
53. Guan C, Zou X, Shi W, Gao J, Yang C, Ge Y, Xu Z, Bi S and Zhong X: Metallothionein 1B attenuates inflammation and hepatic steatosis in MASH by inhibiting the AKT/PI3K pathway. J Lipid Res 66: 100701, 2025.
54. Laila UE, Zhao ZL, Xu DY, Liu H and Xu ZX: Pharmacological advances and therapeutic applications of niclosamide in cancer and other diseases. Eur J Med Chem 290: 117527, 2025.
55. Park KS, Jo I, Pak K, Bae SW, Rhim H, Suh SH, Park J, Zhu H, So I and Kim KW: FCCP depolarizes plasma membrane potential by activating proton and Na+ currents in bovine aortic endothelial cells. Pflugers Arch 443: 344-352, 2002.
56. Vilar-Gomez E, Martinez-Perez Y, Calzadilla-Bertot L, Torres-Gonzalez A, Gra-Oramas B, Gonzalez-Fabian L, Friedman SL, Diago M and Romero-Gomez M: Weight loss through lifestyle modification significantly reduces features of nonalcoholic steatohepatitis. Gastroenterology 2: 367-378, 2015.
57. Wilding JP: The importance of weight management in type 2 diabetes mellitus. Int J Clin Pract 68: 682-691, 2014.
58. Neeland IJ, Linge J and Birkenfeld AL: Changes in lean body mass with glucagon-like peptide-1-based therapies and mitigation strategies. Diabetes Obes Metab 26 (Suppl 4): S16-S27, 2024.
59. Cava E, Yeat NC and Mittendorfer B: Preserving healthy muscle during weight loss. Adv Nutr 8: 511-519, 2017.
60. Hardie DG, Ross FA and Hawley SA: AMPK: A nutrient and energy sensor that maintains energy homeostasis. Nat Rev Mol Cell Biol 13: 251-262, 2012.
61. Tai T, Shao YY, Zheng YQ, Jiang LP, Han HR, Yin N, Li HD, Ji JZ, Mi QY, Yang L, *et al*: Clopidogrel ameliorates High-fat diet-induced hepatic steatosis in mice through activation of the AMPK signaling pathway and beyond. Front Pharmacol 15: 1496639, 2024.
62. Wang Y, Liu S, Ni M, Chen Y, Chen R, Wang J, Jiang W, Zhou T, Fan S, Chang J, *et al*: Terf2ip deficiency accelerates non-alcoholic steatohepatitis through regulating lipophagy and fatty acid oxidation via Sirt1/AMPK pathway. Free Radic Biol Med 220: 78-91, 2024.
63. Matsusue K, Haluzik M, Lambert G, Yim SH, Gavrilova O, Ward JM, Brewer B Jr, Reitman ML and Gonzalez FJ: Liver-specific disruption of PPARgamma in leptin-deficient mice improves fatty liver but aggravates diabetic phenotypes. J Clin Invest 111: 737-747, 2003.
64. Baumann A, Burger K, Brandt A, Staltner R, Jung F, Rajcic D, Lorenzo Pisarello MJ and Bergheim I: GW9662, a peroxisome proliferator-activated receptor gamma antagonist, attenuates the development of non-alcoholic fatty liver disease. Metabolism 133: 155233, 2022.
65. Sozio MS, Lu C, Zeng Y, Liangpunsakul S and Crabb DW: Activated AMPK inhibits PPARα and PPARγ transcriptional activity in hepatoma cells. Am J Physiol Gastrointest Liver Physiol 301: G739-G747, 2011.
66. Blanchard PG, Festuccia WT, Houde VP, St-Pierre P, Brûlé S, Turcotte V, Côté M, Bellmann K, Marette A and Deshaies Y: Major involvement of mTOR in the PPARγ-induced stimulation of adipose tissue lipid uptake and fat accretion. J Lipid Res 53: 1117-1125, 2012.
67. Hunter CA, Kartal F, Koc ZC, Murphy T, Kim JH, Denvir J and Koc EC: Mitochondrial oxidative phosphorylation is impaired in TALLYHO mice, a new obesity and type 2 diabetes animal model. Int J Biochem Cell Biol 116: 105616, 2019.
68. Xiong G, Zhang K, Ma Y, Song Y, Zhang W, Qi T, Qiu H, Shi J, Kan C, Zhang J and Sun X: BAM15 as a mitochondrial uncoupler: A promising therapeutic agent for diverse diseases. Front Endocrinol (Lausanne) 14: 1252141, 2023.
69. Yoo HC, Yu YC, Sung Y and Han JM: Glutamine reliance in cell metabolism. Exp Mol Med 52: 1496-1516, 2020.
70. Amores-Sánchez MI and Medina MA: Glutamine, as a precursor of glutathione, and oxidative stress. Mol Genet Metab 67: 100-105, 1999.
71. Torres N, Tobón-Cornejo S, Velazquez-Villegas LA, Noriega LG, Alemán-Escondrillas G and Tovar AR: Amino acid catabolism: An overlooked area of metabolism. Nutrients 15: 3378, 2023.
72. TeSlaa T, Ralser M, Fan J and Rabinowitz JD: The pentose phosphate pathway in health and disease. Nat Metab 5: 1275-1289, 2023.
73. Dungubat E, Kusano H, Mori I, Tawara H, Sutoh M, Ohkura N, Takanashi M, Kuroda M, Harada N, Udo E, *et al*: Age-dependent sex difference of non-alcoholic fatty liver disease in TSOD and db/db mice. PLoS One 17: e0278580, 2022.
74. Chen SY, Beretta M, Olzomer EM, Alexopoulos SJ, Shah DP, Byrne FL, Salamoun JM, Garcia CJ, Smith GC, Larance M, *et al*: Head-to-head comparison of BAM15, semaglutide, rosiglitazone, NEN, and calorie restriction on metabolic physiology in female db/db mice. Biochim Biophys Acta Mol Basis Dis 1870: 166908, 2024.